# AN EXPLORATORY INVESTIGATION OF A FREE FALL SUBMERSIBLE ESCAPE CAPSULE FOR AN OFFSHORE OIL RIG



RAJU GOTETI

# AN EXPLORATORY INVESTIGATION OF A FREE FALL SUBMERSIBLE ESCAPE CAPSULE FOR AN OFFSHORE OIL RIG

by

© Raju Goteti, B.Tech.

A thesis submitted to the School of Graduate Studies in partial fulfillment of the requirements for the degree of Master of Engineering

Faculty of Engineering
Memorial University of Newfoundland

September 1988

St. John's Newfoundland

ISBN 0-315-50462-5

To my parents

## ABSTRACT

The Ocean Ranger and other oil rig disasters have shown that rig evacuation systems often do not work properly during severe storms. Most make use of cables to lower the survival craft to the ocean surface. In stormy weather, a pendulum-like motion of the craft can develop causing it to crash into the rig structure. Even when a craft reaches the ocean surface intact, high winds and waves can drive it against rig structures near the waterline. A free fall submersible capsule system is proposed in this thesis which could avoid these problems. Upon release from the rig, the capsule would fall freely to the ocean surface. It would then sink into the ocean down to a level where water motion is insignificant.

Obviou sly, there are many factors that would have to be considered for a complete investigation of such a system. Some of these are: the release mechanism, the free fall in gale force winds, the impact of the capsule onto the ocean surface, the post impact trajectory beneath the surface, the capsule recovery and the life support systems. This thesis examines only the impact and control aspects of the evacuation. Experimental data are presented which show that the decelerations experienced by a capsule when it impacts the ocean surface are well within human tolerance limits. Also, experimental data are presented which show that at

model scale the submergence depth of a capsule can be adequately controlled. This is in spite of the fact that the model constructed had severe hardware limitations. Obviously, with better hardware, much better control should be possible. The describing function concept of classical control theory explained much of what was seen in the depth control experiments.

ACKNOWLEDGEMENTS

I wish to thank my supervisor, Dr. M.J. Hinchey, for his support and guidance during my studies at MUN and for suggesting the submergence escape capsule as a thesis topic. I also wish to thank Dr. J.J. Sharp for his valuable suggestions with regard to impact scaling. I appreciate very much the encouragement and financial support provided by the School of Graduate Studies at MUN. I thank Dr. T.R. Chari, Dr. G.R. Peters and Dr. F.A. Aldrich in this regard. Technicians A. Bursey and R. O'Driscoll and wave tank staff M. Sullivan and B. Wilkie were extremely helpful during the experimental part of my work. Finally, I must also thank my colleague Deb Sen for his helpful suggestions and Mrs. Mary Brown for typing the manuscript.

# TABLE OF CONTENTS

## Nomenclature

### Roman

| | |
|---|---|
| A | Magnitude of Output from Relay |
| a | Impact Deceleration |
| C | Sound Speed in Water |
| $C_d$ | Drag Coefficient |
| c | Damping Coefficient |
| D | Capsule Diameter |
| d | Deadband |
| E | Limit Cycle Amplitude |
| $F_B$ | Buoyancy Force |
| $F_C$ | Control Force |
| $F_D$ | Drag Force |
| $F_G$ | Gravitational Force |
| $F_M$ | Added Mass Force |
| $F_R$ | Froude Number (H/D) |
| FR | Flow Rate (CFM) |
| $G_L$ | Linear Element in Forward Path |
| g | Acceleration due to Gravity |
| H | Drop Height |
| $I_{DF}$ | Input into Describing Function |
| $I_N$ | Input into Nonlinear Controller |
| j | $\sqrt{-1}$ |
| K | Gain |
| M | Mach Number (U/C) |
| M | Mass of Sphere |
| $M_W$ | Mass of Water displaced by Capsule |
| m | Capsule Mass |

| | |
|---|---|
| $N$ | Describing Function ($O_{DF}/I_{DF}$) |
| $N_{KC}$ | Keulegan-Carpenter Number ($UT/D$) |
| $O_{DF}$ | Output from Describing Function |
| $O_N$ | Output from Nonlinear Controller |
| $O_o$ | Fundamental Output from Nonlinear Controller |
| Re | Reynolds Number ($UD/\nu$) |
| SR | Sampling Rate |
| s | Laplace Variable |
| T | Flow Oscillation Period |
| t | Time |
| U | Impact Speed |
| Z | Submergence Depth |

Greek

| | |
|---|---|
| $\Delta$ | Density Ratio ($\rho_c/\rho_W$) |
| $\lambda$ | Root of System Characteristic Equation |
| $\nu$ | Kinematic Viscosity of Water |
| $\pi$ | 3.14159 ... |
| $\rho_W$ | Density of Water |
| $\rho_C$ | Density of Capsule |
| $\omega$ | Radian Frequency |

Subscripts

| | |
|---|---|
| m | Model |
| o | Initial Condition |
| p | Prototype |

## List of Figures

# 1. INTRODUCTION

## 1.1 Background

The Ocean Ranger and other oil rig disasters have shown that in severe storms rig evacuation systems are often inadequate [Ocean Ranger Royal Commission Report 1984]. Typically, during the deployment of a lifeboat, it is often damaged to the point of not being seaworthy before it reaches the ocean surface. Even when a lifeboat does manage to get to the ocean surface intact, high winds and waves often drive it against structures near the water line. Although improvements in this regard have been recently developed, evacuation systems for offshore oil rigs are still far from being satisfactory. It is obvious that much more work needs to be done in this area, especially for the Canadian East Coast area where the storms can be extremely severe and the waters can be ice infested.

## 1.2 Evacuation Systems Review

Evacuation systems currently in use on oil rigs offshore can be divided into three categories: dry systems, semi-wet systems and wet systems [Muggeridge, 1985].

Dry evacuation systems are generally not used when weather conditions are rough. As the name implies, these

systems generally do not make direct contact with the ocean. The most commonly used dry system is the helicopter. Several factors restrict its use. Some of these are: high wind speed, poor visibility, unsteady orientation of the rig's helideck, combustible gas or fire on the rig and distance to the nearest safe haven. If there is a vessel on standby near the rig, then crane held baskets or nets can sometimes be used to transfer personnel directly to it. This is also a dry system. Sometimes a cable can be secured between the rig and the vessel. In this case, personnel can slide along this to safety.

At the other extreme is the wet system. A good example of this is the thermal suit. This is normally used as a last resort. Unfortunately, during the Ocean Ranger disaster, personnel were not equipped with such suits so once in the water they quickly succumbed to the bitter cold.

The conventional lifeboat is a good example of the semi-wet system, and it is the most commonly used method of evacuation during severe storms. Typically, the boats are totally enclosed and they are lowered on cables slowly to the ocean surface. In stormy weather, a pendulum-like motion of the boat on the cables can develop causing it to crash into the rig structure. A number of accidents of this nature have been reported [Muggeridge, 1985]. Even when a lifeboat manages to reach the ocean surface intact, it can

be driven by the force of winds and waves against structures near the water-line.

A new semi-wet system was recently developed which is claimed to have overcome the near water-line problem [Boyd, 1984]. This system is known as the Preferred Orientation and Displacement (PROD) system, and it is designed to be easily retrofitted to existing platforms. The key element of the PROD system is a long flexible boom. This is attached to the bow of the survival craft by means of a line known as the tag line, as illustrated in Figure 1. The length of both the boom and the tag line are roughly equal to the height of the stowed survival craft above the water line. As the craft is lowered to the water surface, the boom bends. When the craft touches the water surface, the rear line disconnects, and the boom begins to straighten. As it straightens, the energy stored in it is released, and this gives the craft a motion away from the rig. This system is now in use offshore. However, it has never been tested in extreme weather conditions.

Freefall lifeboats do not use cables and so avoid some of the problems of cable-launch systems. Such systems were developed in Norway by the Norwegian Maritime Directorate following two disasters which occurred to the ships 'Anita' and 'Norse Variant'. The lifeboats on these ships were damaged before they could reach the ocean surface. Most of

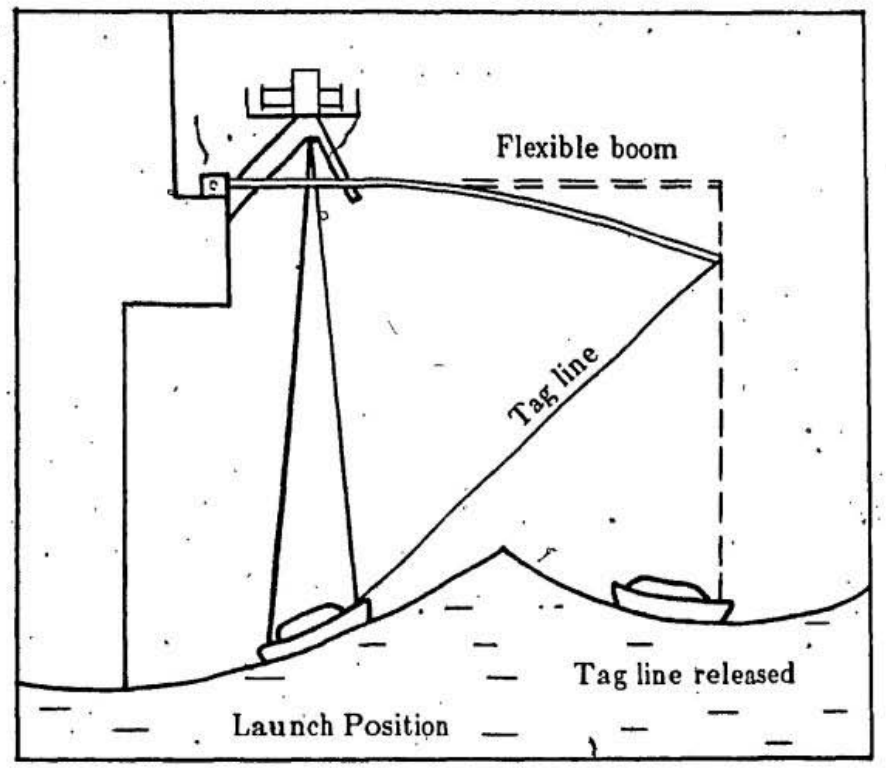


Figure 1 PROD System.

the personnel onboard died as a result of this. A skid-launched boat called 'Tarcoola', having a capacity of 400 persons, was developed in the period 1972-1978. This was developed for use on large vessels where the point of release of the lifeboat was typically 20 meters above the ocean surface. A drop-launched steel boat called 'SSB' was developed for use on offshore structures in the period 1979-1983 [Werenskiod, 1983]. This lifeboat was designed for a seating capacity of 75 persons and a maximum drop height of 30 meters. Free fall systems impact the water surface at high speed and subject the personnel onboard to decelerations around 10 g for a short period of time. Obviously, the personnel onboard and the craft itself must be able to withstand these decelerations. Also, the post-impact trajectory is a potentially serious problem. High winds and waves can drive the boat against structures near the water-line. Skid-launched free-fall systems are designed to counteract this. Finally, personnel are hesitant to get into a system which falls freely for 25 m, so free-fall systems are subject to this psychological factor as well.

## 1.3 Scope of Project

In this thesis, a new semi-wet evacuation system is proposed. The system will be referred to as the free-fall submersible escape capsule. Upon release from a rig, such a capsule would fall freely to the ocean surface. It would then sink into the ocean. Water motions are insignificant at a wave length or so below the surface. So, by sinking into the ocean, a capsule could avoid the violent air and water motions near the surface. Figure 2 shows what a prototype capsule might look like. Some rough calculations suggest that a spherical capsule 4.5 m in diameter would be able to hold 50 people. For scaling purposes, we will consider this to be the prototype size.

A complete investigation of such a system is beyond the scope of the present work. For a complete investigation, one would have to consider, among other things: the release mechanism, the free fall in gale force winds, the impact of the capsule onto the ocean surface, the post impact trajectory beneath the surface, hydrostatic stability, the capsule recovery and the life support systems. Here, only the impact and control aspects are considered.

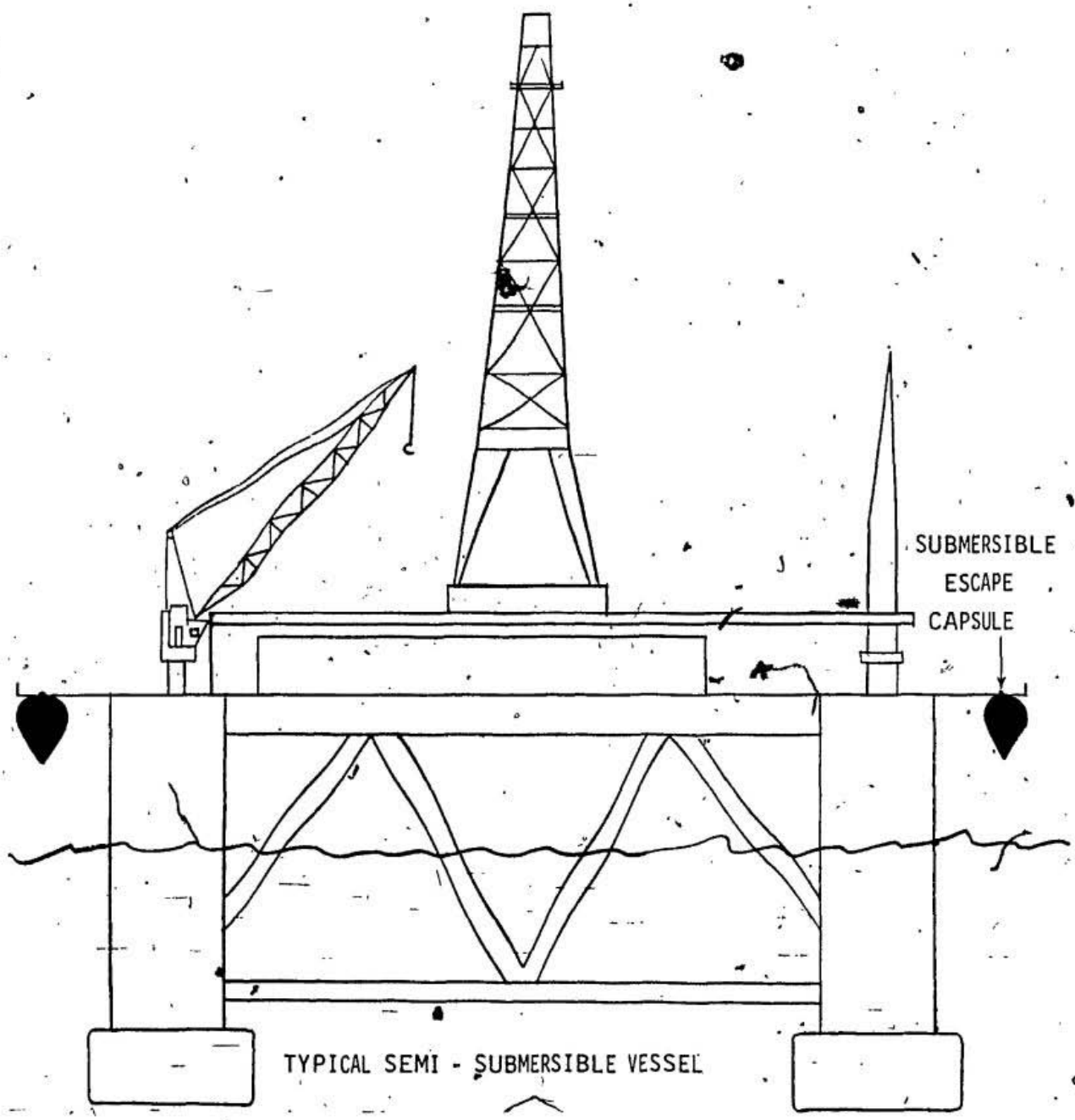


Figure 2 Submersible Escape Capsule.

# 2. CAPSULE-WATER IMPACT

## 2.1 Background

When a capsule impacts onto the ocean surface, it decelerates quickly. In previous work on free-fall lifeboats, decelerations as high as 10 g were reported. We expect the impact decelerations for a submersible capsule to be much lower. This is because a submersible capsule is more massive than the corresponding floating system. This gives it greater impact momentum. Below, impact decelerations for a simple spherical capsule were studied experimentally.

## 2.2 Impact Review

The impact of objects onto a water surface has been a subject of interest for many years. The earliest reports on the phenomenon were by Worthington and Cole [1897]. They reported on splashes caused by spheres free-falling onto a water surface. Model testing of re-entry capsules was initiated in 1959 as part of NASA's space program. Impact studies were conducted by V.L. Vaughan [1959] for three models each with a different shape. These are shown in Figure 3. A linear relationship was observed between the impact speed squared and model deceleration, for each of the three models tested. As will be shown later, this result

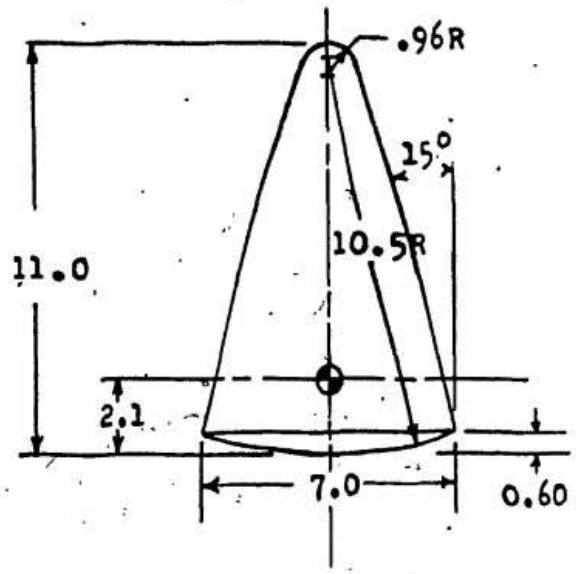


MODEL A (SPHERICAL BOTTOM)

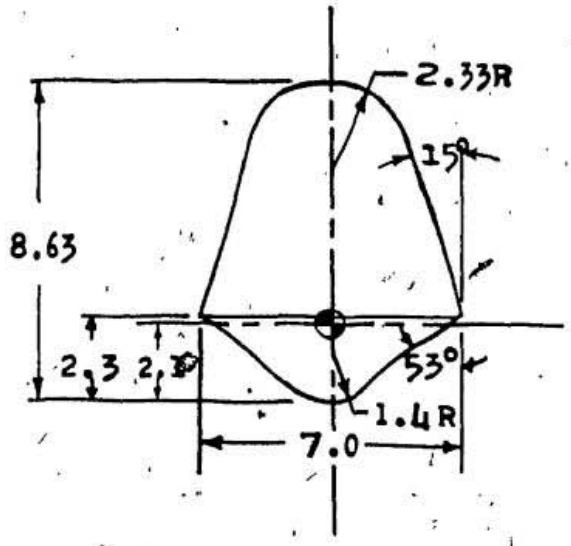


MODEL B (CONICAL BOTTOM)

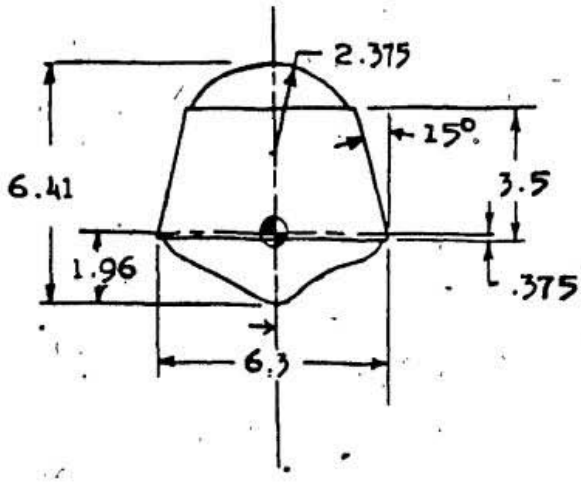


MODEL C (CONVEX-CONCAVE BOTTOM)

DETAILS OF MODELS. (DIMENSIONS ARE FULL SCALE IN FEET)

**Figure 3 Re-Entry Capsule Geometries.**

suggests that the impact flows are inertia dominated and the Froude Number $U^2/gD$ is the appropriate scaling parameter, where U is the impact speed, g is the acceleration due to gravity and D is the characteristic dimension of the body. Baker, Westine and Dodge [1973] did an extensive series of impact tests on the Apollo Command Module (Figure 4) and came to a similar conclusion with regard to scaling.

Some attempts at studying the impact phenomenon theoretically have been reported. Some are based on potential flow concepts [Li and Sigimura, 1967] while others are based on the Navier Stokes equations [Nichols, Hirt and Hotchkiss, 1980]. These are beyond the scope of the present work.

## 2.3 Scaling

During an impact, there are several flow phenomena that could be potentially important.

As a capsule nears the surface, the motion of the air directly beneath it will induce some water motion. However, if this effect is small, the water near the point of contact will undergo a shock phase. For this, the compressibility of the water is important because it determines how fast pressure waves can propagate in the form of shock waves throughout the water. The important dimensionless parameter

All dimensions are in inches.

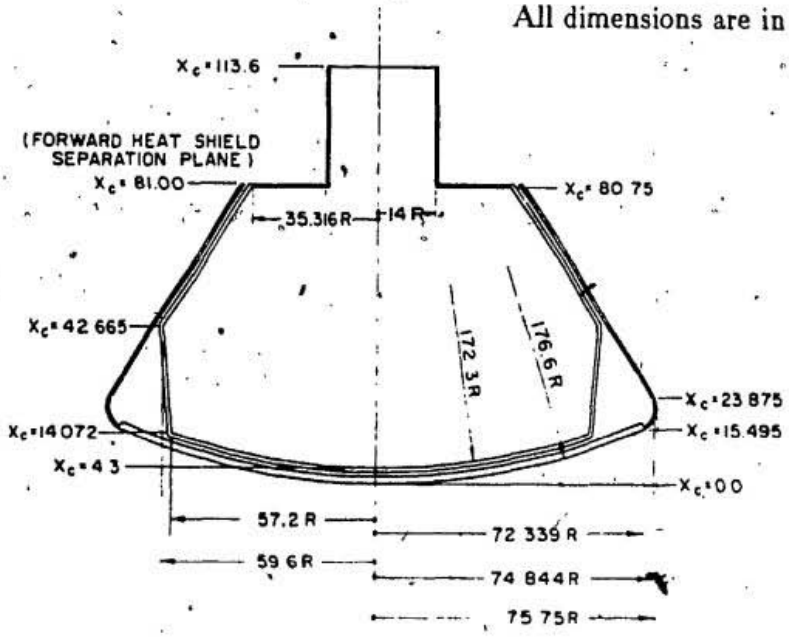


Figure 4 Apollo Command Module.

is the Mach number M given by:

$$M = \frac{U}{C} \tag{2.1}$$

where U is the impact speed and C is the sound speed in water. During the shock phase, very high pressures are usually generated. However, they act for a short period of time over a small area and they have been found not to contribute significantly to a capsule's deceleration.

Immediately after the shock phase, the flow would be inertia dominated. Here, the water directly in front of the body has to be moved laterally. The important dimensionless parameter for this phase is the Froude number $F_R$ given by

$$F_R = \frac{U^2}{gD} \tag{2.2}$$

where g is the acceleration due to gravity and D is the characteristic dimension of the body. Now, for a falling body, the impact speed U will be given approximately by:

$$U = \sqrt{gH} \tag{2.3}$$

where H is the drop height. Substitution of this into the expression for $F_R$ gives

$$F_R = \frac{gH}{gD} = \frac{H}{D} \qquad (2.4)$$

$$F_R^* = \frac{H}{D}$$

From previous work, one could expect this parameter to have a large influence on a capsule's deceleration.

If a capsule has an average density $\rho_c$ which is greater than the density of water $\rho_w$, it will sink into the water, wakes will form behind it and there will be a transition from inertia to viscosity dominated flow. In other words, there will be a transition from Froude number to Reynolds number scaling where the Reynolds number Re is given by:

$$Re = \frac{UD}{\nu} \qquad (2.5)$$

where $\nu$ is the kinematic viscosity of water. For floating capsules, viscous phenomena have been found to be insignificant. For submersible capsules, this may not be the case.

For a particular geometry, an application of the Buckingham $\pi$ theorem gives

$$\frac{a}{g} = \text{ftn } (M, F_R^*, Re, \Delta) \qquad (2.6)$$

where $\Delta = \rho_c / \rho_w$. From previous work, one would expect this to reduce to

$$\frac{a}{g} = \text{ftn } (F_R^*, \Delta) \qquad (2.7)$$

## 2.4 Capsule Drop Tests

### 2.4.1 Setup

Spherical models, constructed mainly from wax, some 0.3 m in diameter and some 0.15 m in diameter, were dropped from various heights into the MUN Deep Tank, which is approximately 4 m by 4 m by 4 m. Styrofoam and steel weights were used to adjust the density ratio of each model. The smaller model had a geometric scaling factor of 1:30 while the larger one had a scaling factor of 1:15.

The impact deceleration was sensed using a Bruel and Kjaer 4344 accelerometer, together with a Bruel and Kjaer 2626 conditioning amplifier. The accelerometer, with its sensing axis aligned with the vertical, was embedded into each sphere prior to testing. Signals from it were recorded on magnetic tape. They were later processed using a Hewlett

Packard 5420B Digital Signal Analyzer. Figure 5 shows a schematic of the test setup.

### 2.4.2 Data and Discussion

Figure 6 shows a typical acceleration versus time plot obtained from the experiments. Just after the model was released, the accelerometer picked up the 1 g free fall acceleration. This is denoted by the letter A in the plot. When impact occurred, there was a rapid deceleration, and this is denoted by the letter B. A string attached to the model was used to keep it from sinking to the bottom of the tank. When this became taut, the complicated signal denoted by the letter C was produced. Each experiment was repeated three times and the plots generated showed a high degree of consistency.

Figure 7 shows the acceleration data obtained from the experiments. As can be seen, for each model, the relationship between a/g and H/D is linear. Also, the data for the larger model are consistent with that of tthe smaller model. This suggests that Froude number scaling is appropriate. The data show that for a given H/D the impact decelerations increase as the density ratio $\Delta$ is reduced. This is not surprising. As $\Delta$ tends to zero, the momentum of the impacting body also tends to zero. Thus, in this limit, the body cannot move the water and so its a/g must tend to infinity.

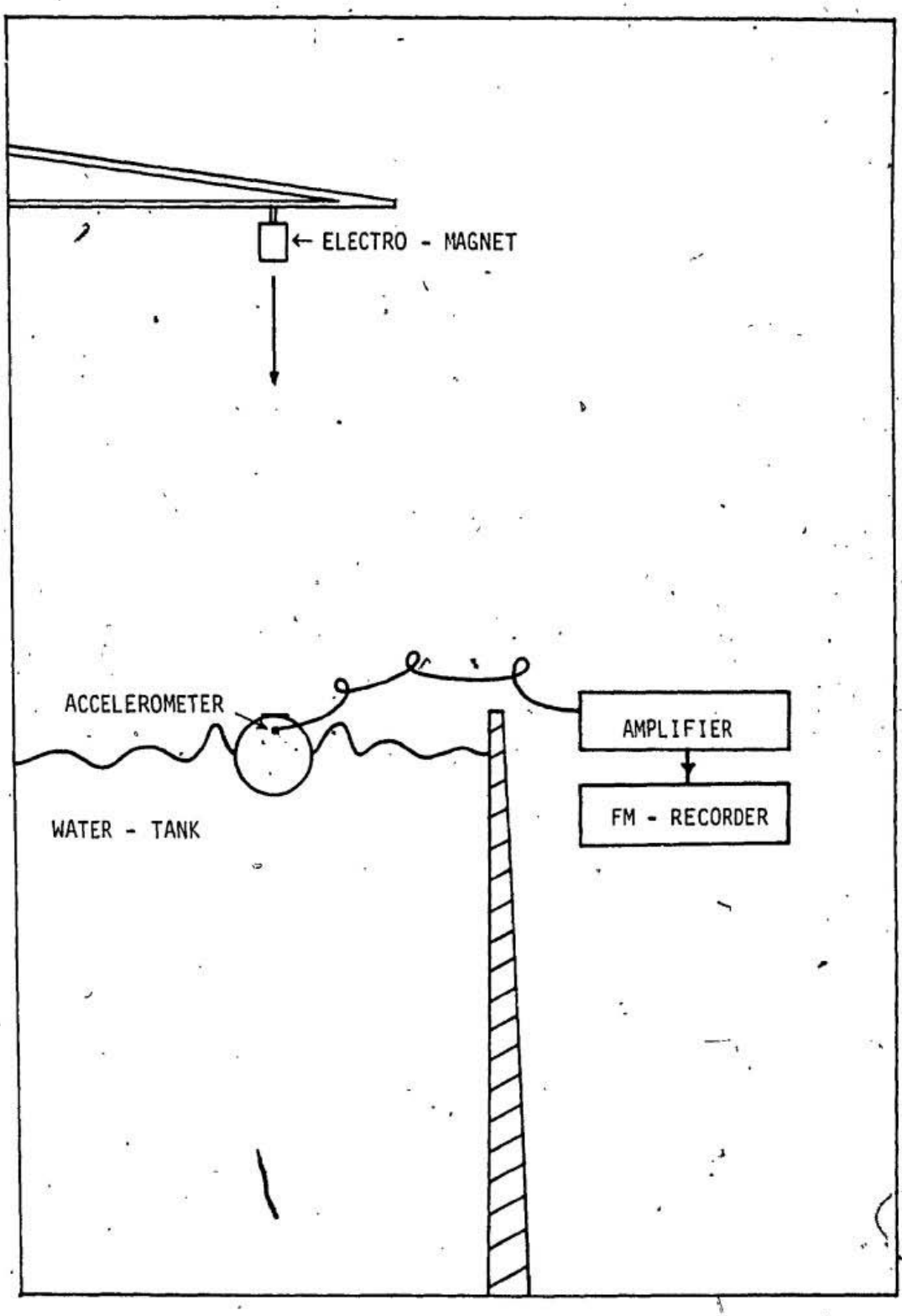


Figure 5 Impact Test Setup.

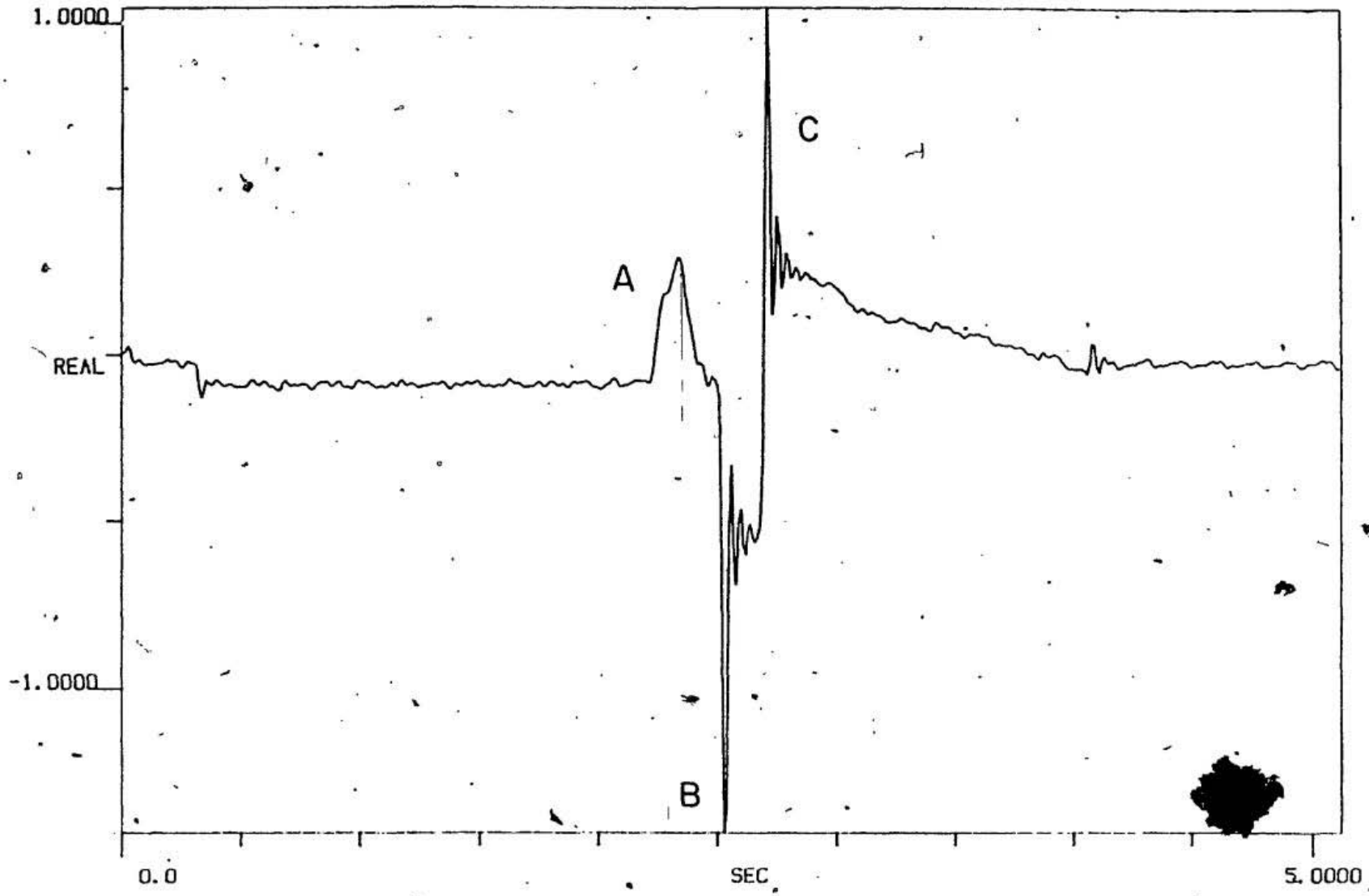


Figure 6 Typical Impact Signal from Accelerometer.

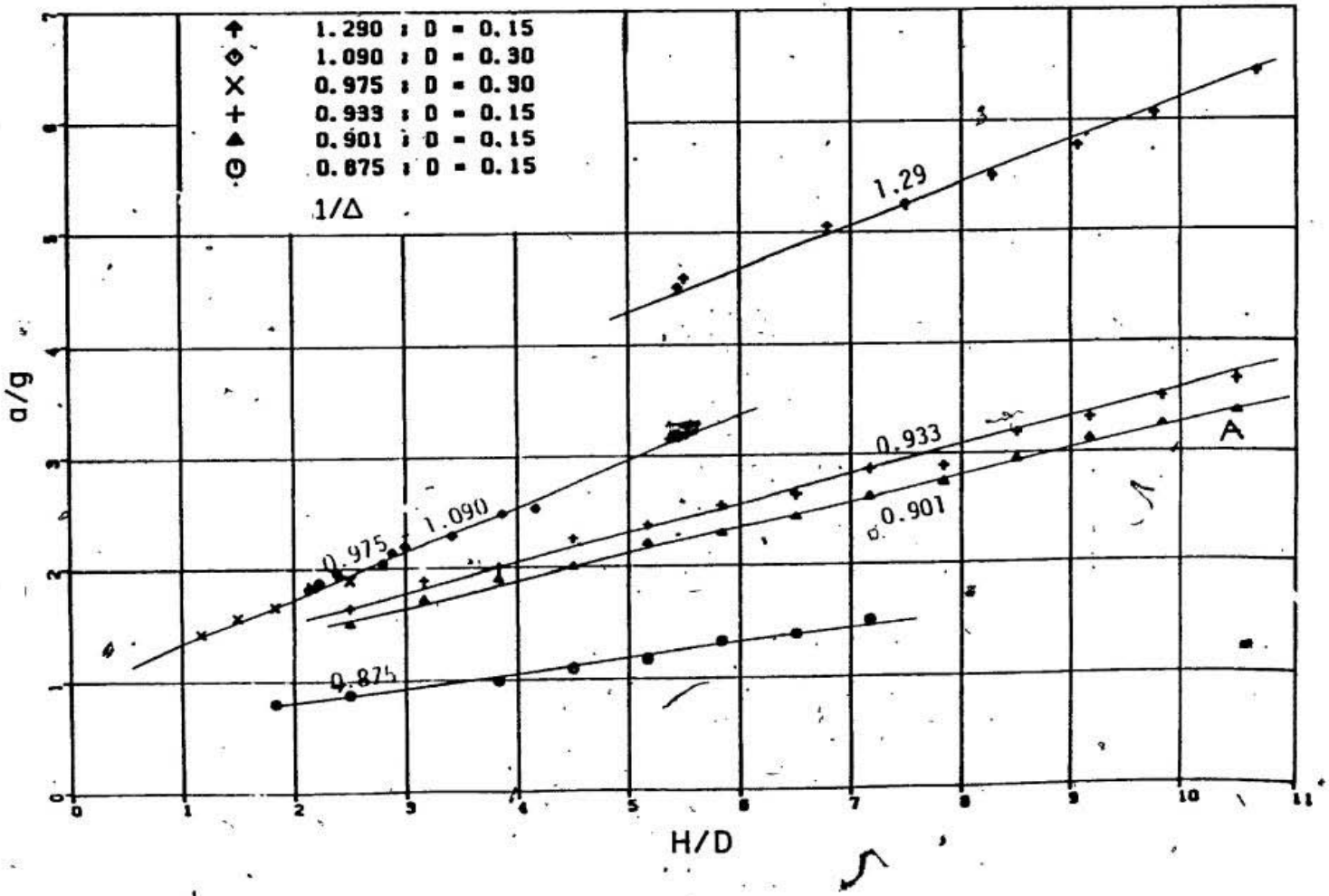


Figure 7 Nondimensional Impact Deceleration versus Nondimensional Drop Height.

When considering the effect of an impact on people inside a capsule, the number of g's is obviously an important factor. However, the duration of the impact is also important. For an impact of a free-fall lifeboat lasting 0.2 seconds, the upper limit on deceleration used in design is 10 g [Research Institute of Norway]. For shorter durations the upper limit is higher. From Figure 7, one can see that for a submersible capsule the decelerations would always be below 5 g. Figure 6, which is for the smaller model and corresponds to the point labelled A in Figure 7, shows that the shortest impact duration T for it is about 0.04 seconds. For an impact governed by Froude scaling, one can show that

$$\frac{T_p}{T_m} = \sqrt{\frac{D_p}{D_m}} \qquad (2.8)$$

where p and m indicate the prototype and the model respectively. Substitution into this gives $T_p$=0.2 seconds approximately. So, it appears that the impact decelerations would not be a problem. In fact, the g level felt onboard a prototype would probably be much less than that reported here. The present investigation ignored the elastic and damping properties of the capsule and the seat padding and supports. These factors should isolate the people onboard from the impact and subject them to a lower g level.

# 3. SUBMERGENCE DEPTH CONTROL

## 3.1 Background

When a capsule sinks beneath the ocean surface, its trajectory must be controllable. This includes both the submergence depth and the motion in the horizontal plane. For the present work, we concentrated on submergence depth only. The submergence depth could be controlled manually. However, in an emergency situation, this would be extremely risky. Thus, during normal operation, the control system would have to be automatic, requiring little or no human intervention. The control system components could all be analog devices. However, a hybrid system composed of analog and digital components would be much more flexible. For example, a digital computer could receive a signal from some depth sensor and thus sense the depth error. It could then process this and send out a signal to take corrective action. This is the approach taken here. The use of a digital computer to take corrective action means that many control strategies are possible.

Our goal was to show that we could construct a model of the submersible capsule and control its submergence depth. Unfortunately, the model constructed suffered from severe hardware limitations. In a prototype, the depth could be controlled by using an onboard supply of compressed air to

control the capsule's buoyancy. At model scale, this was difficult to do, and we ended up using an external air supply. A long hose was used to connect the model to this supply. The complex flow within this was extremely difficult to model theoretically.

The physical model is shown schematically in Figure 8. As can be seen, it is spherical in shape, and it has a central chamber which is closed on top but open on the bottom. The density ratio $\Delta$ of the model was controlled by a flow of air into or out of this chamber. When the chamber is completely filled with water $\Delta$=1.05 while when it is completely filled with air $\Delta$=0.95. An ASCO 8314C15 solenoid valve in the air supply line was used to regulate the flow. This is basically an ON-OFF device: when ON air flowed from the supply line into the chamber whereas when OFF air flowed from the chamber to atmosphere. A Druck PCDR 81 pressure transducer was used to sense the submergence depth.

An IBM PC-XT digital computer together with a Keithley 570 Data Acquisition System and an advanced BASIC software package known as SOFT 500 [Keithley 1984] was used to sense the depth error and take corrective action on-line. It took in the signal from the pressure transducer, converted it to a digital form and then used it to determine the depth error at specific instants in time. It gave out a control signal based on the error. This activated a Potter and Brumfield

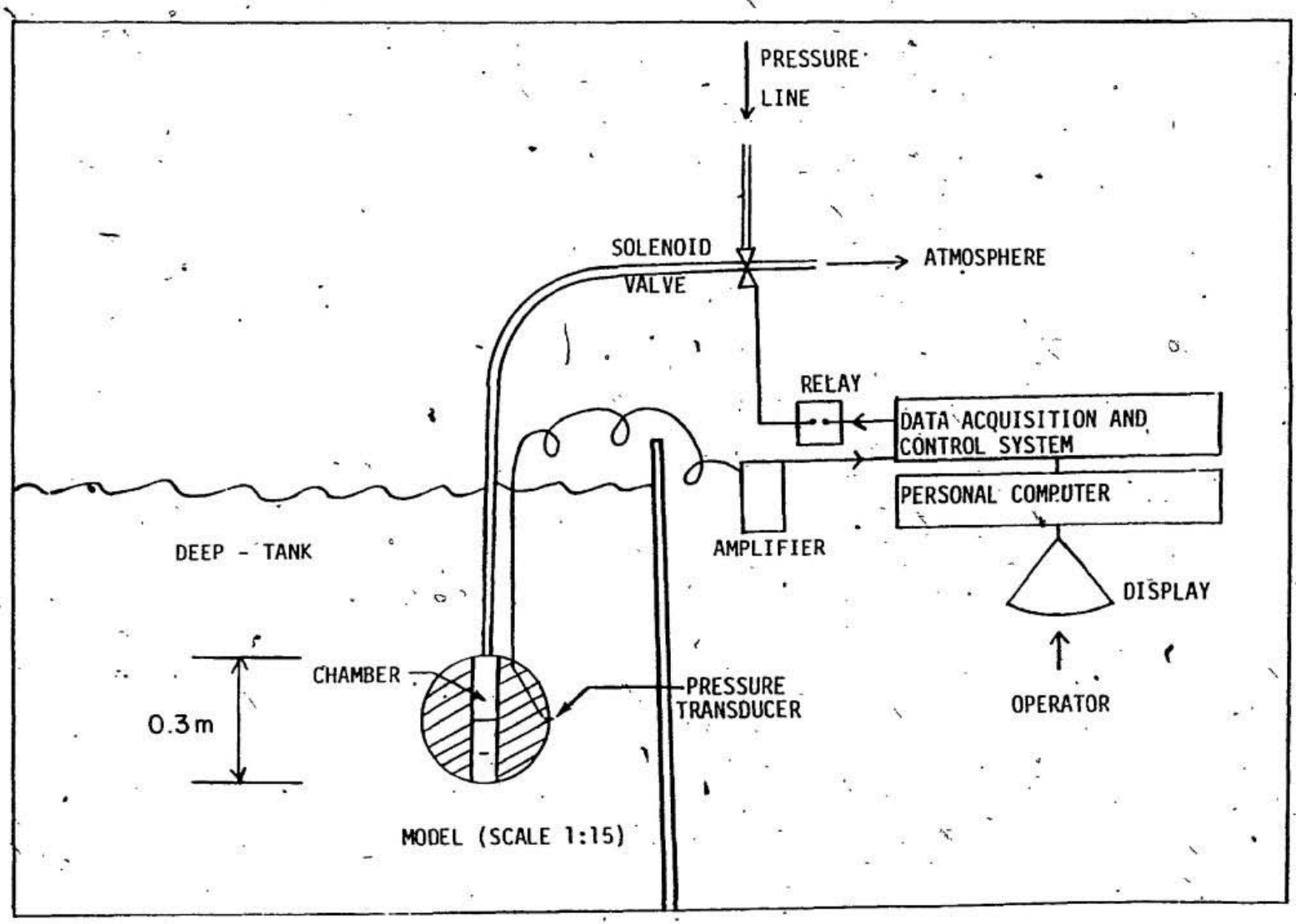


Figure 8 Depth Control Setup.

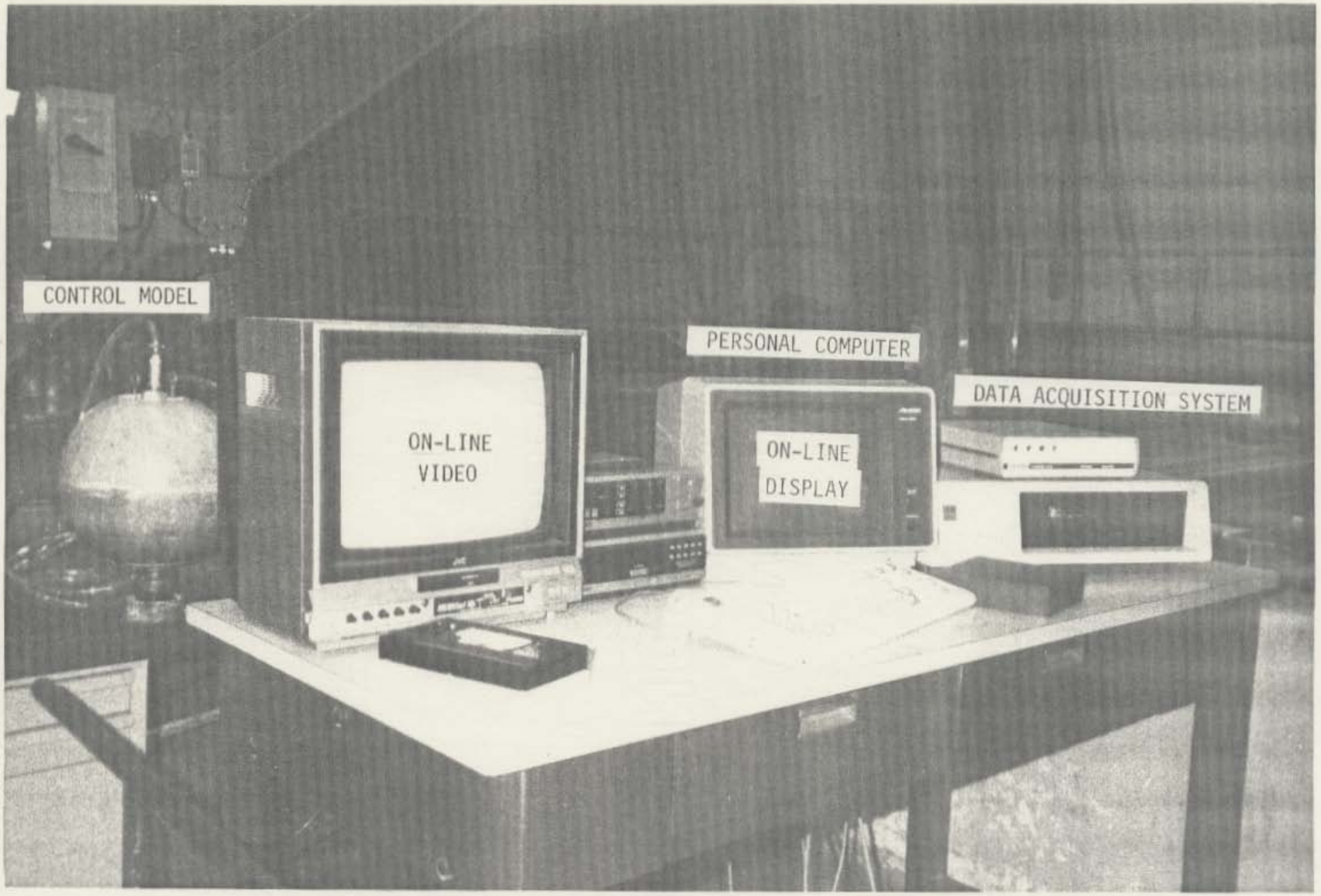
CONTROL MODEL
ON-LINE
VIDEO
PERSONAL COMPUTER
ON-LINE
DISPLAY
DATA ACQUISITION SYSTEM

EOM-IDA72-3/32 relay in the solenoid valve assembly and, as mentioned previously, this regulated the flow of air.

Two control strategies were chosen for the present work. Their SOFT 500 programs are given in an Appendix to this report. The objective of each was to make the physical model hover 2 m below the water surface in the MUN deep tank. In the prototype, this corresponds to a submergence depth of 30 m. In the first, the controller sent airflow into the model when the depth was below 2 m and allowed air to vent to atmosphere when the model was above 2 m. In the second, the model's direction of motion within a depth range centered around the desired depth was taken into consideration. Outside this range, air was sent into the model when the depth was below the range and was allowed to vent to atmosphere when the depth was above the range. Within the range, air was supplied to the model when it was moving downward and it was vented to atmosphere when the model was moving upward.

## 3.2 Theoretical Formulation

Because of the ON-OFF nature of its controller, the system being considered is inherently nonlinear. One could integrate the governing equations of the system to study its behaviour. This is fairly straightforward, and we did this here. We also used the describing function concept of

classical control theory [Harrison and Bollinger 1969]. This approach gives greater insight into the system's performance.

### 3.2.1 Governing Equations

For the motion of a sphere moving vertically in water, the governing equation is Newton's Second Law. The forces acting on the sphere are the gravitational force $F_G$, the buoyancy force $F_B$, the added mass force $F_H$ and the viscous drag force $F_D$.

The gravitational force is

$$F_G = Mg \tag{3.1}$$

where M is the mass of the sphere and g is the acceleration due to gravity. The positive direction is taken to be vertically downward from the water surface.

The buoyancy force is

$$F_B = -M_W g \tag{3.2}$$

where $M_W$ is the mass of displaced water. This is controlled by the amount of air in the central chamber.

The added mass force accounts for the fact that an accelerating sphere accelerates the water around it and because of this it appears to be more massive. This force is given approximately by [Lamb 1932]:

$$F_M = \frac{-M_w}{2} \frac{dU}{dt} \tag{3.3}$$

where U is the velocity of the sphere.

The viscous drag is made up of two components: skin friction and wake drag. If the flow over the sphere behaves quasi-statistically, then the viscous drag at any instant in time is given approximately by

$$F_D = -\frac{\rho_w}{2} U|U| \frac{\pi D^2}{4} C_d \tag{3.4}$$

where $C_d$ is a drag coefficient. Here, we assume quasi-static flow. The Keulegan-Carpenter number tells if a flow is behaving quasi-statically. For a sphere, this is given by

$$N_{KC} = \frac{UT}{D} \tag{3.5}$$

where, for a body undergoing an oscillation, T is the period

of the oscillation. For quasi-static flow, $N_{KC}$ should be greater than 15. Unfortunately, for the present work, this was not always the case. So, the theoretical formulation is somewhat suspect. However, we expect the errors due to this to be reasonable. The modelling of the flow into and out of the central chamber would probably introduce greater errors.

For a given shape, $C_d$ is a function of the Reynolds number Re. Figure 9 shows a typical experimental curve of $C_d$ versus Re for a spherical body [Goldstein 1938]. For the present work, this curve was approximated by the broken line segments shown. For $Re \leq 1$, the Stokes formula $C_d = 24/Re$ was used. For the line segment ab, we used $C_d = 24/Re^{0.646}$. Between points b and c, $C_d$ was set equal to 0.5. The abrupt drop in $C_d$ around $Re = 3 \times 10^5$ indicates a transition from laminar to turbulent flow. For the line segment de, $C_d = 0.000366 \times Re^{0.4275}$ was used. Beyond point e, $C_d$ was set equal to 0.18 [Chow Chuen-Yen 1979].

Taking into consideration all of the above forces, the governing equation of motion is

$$Ma = F = F_G + F_B + F_M + F_D$$

$$M\frac{dU}{dt} = Mg - M_w g - \frac{M_w}{2}\frac{dU}{dt} - \frac{\rho_w}{2}U|U|\frac{\pi D^2}{4}C_d \qquad (3.6)$$

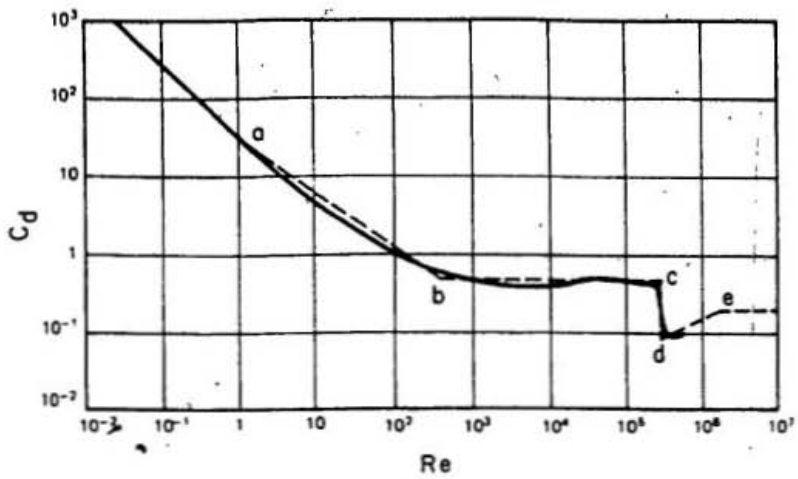


Figure 9 Drag Coefficient versus Reynolds Number for Sphere.

$$\frac{dZ}{dt} = U$$

where Z is the depth of the sphere below the water surface.

### 3.2.2 Classical Control Formulation

As mentioned previously, the controller in the physical model is inherently nonlinear. The viscous drag term in the governing equation is also nonlinear. For the present work, we linearized the latter and used the following simplified form of the governing equation

$$m\ddot{Z} + c\dot{Z} = F_c \tag{3.7}$$

where $F_c$, the control force, is a function of the depth error. The most important requirement of any control system is it should be stable. It should also have reasonable accuracy and speed of response. Here, we concentrate on the stability aspect. We will consider several controllers: some linear and some nonlinear. To examine stability, we will use the Nyquist procedure. Below, we describe this briefly first for linear systems and then for nonlinear systems.

For stable operation of a linear system, each root $\lambda$ of its characteristic equation must be in the left half of the

s plane [Harrison and Bollinger 1969]. In the time domain, each root contributes to a system's response a term like

$$ae^{\lambda t} \qquad (3.8)$$

If each $\lambda$ is a negative real number or has a negative real part, then all transients must decay and the system will be stable. Inspection of the Nyquist Plot for the system shows if there are any roots in the right half of the s plane.

As an illustration, suppose that a proportional controller with gain K could be constructed for a capsule. In this case, the block diagram is as shown in Figure 10. The Nyquist Plot is as shown in Figure 11. It was obtained by setting $s = j\omega$ in the $G_L$ function and plotting the resultant complex number as $\omega$ varied from 0 to $\infty$. The arrow on the curve shows the direction of increasing $\omega$. The plot shows that the system with proportional control is stable because the minus 1/K point is on the left side of the $G_L$ curve. The justification for this statement can be found in any text on automatic control theory [Harrison and Bollinger 1969]. Briefly, for stable operation, the minus 1/K point must not be enclosed by the $G_L$ curve: in other words, it must be outside the curve. Nyquist theory shows that outside is on the left hand side of an observer moving along the $G_L$ curve while inside is on the right hand side.

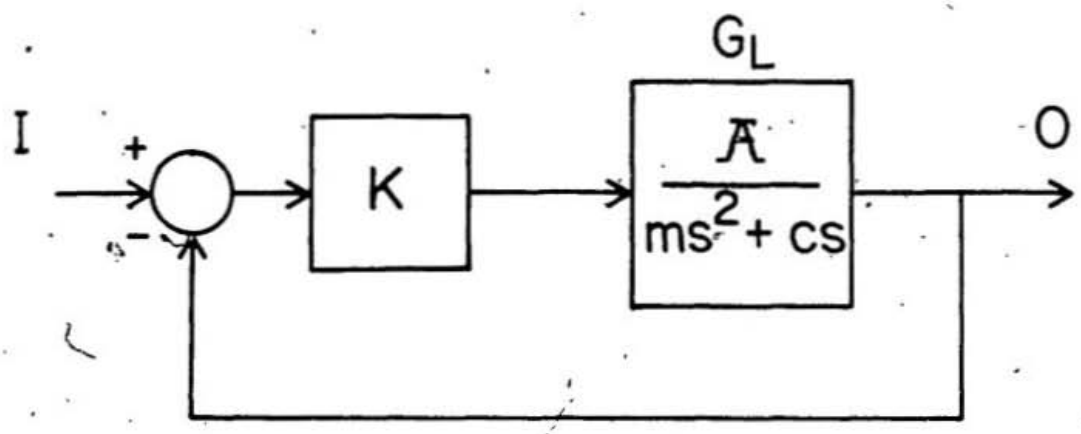


Figure 10 Block Diagram for Capsule with Proportional Control.

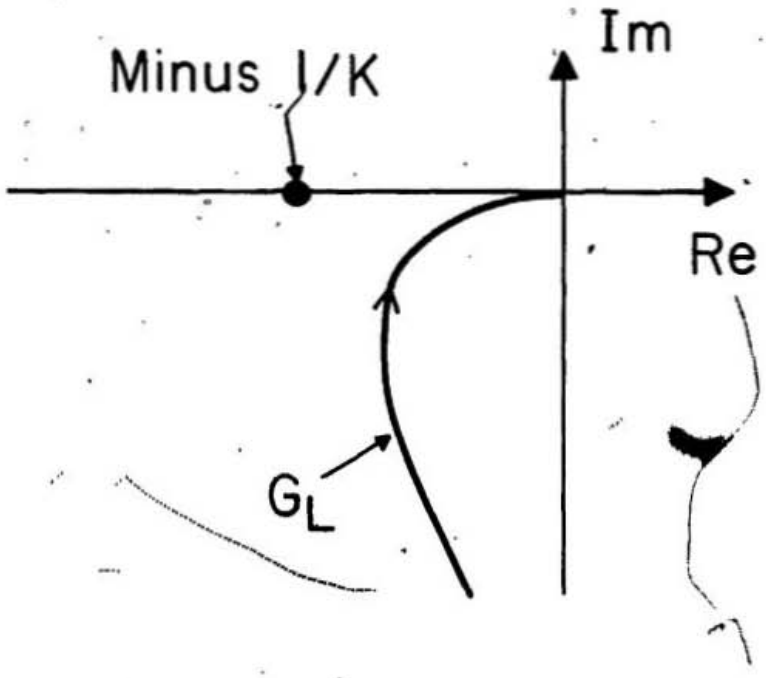


Figure 11 Nyquist Plot for Capsule with Proportional Control.

Suppose now that an integral controller with gain K could also be constructed for the capsule. In this case, the block diagram is as shown in Figure 12 and the Nyquist Plot is as shown in Figure 13. This plot shows that the system with integral control is unstable because the minus 1/K point is on the right side of the $G_L$ curve. So, the integration has degraded stability.

In the physical model, a digital computer is used to sample and reconstruct signals. The rate at which this is done is important. For example, the proportional control case mentioned above can be made unstable if the rate drops below a certain critical level. One can study this phenomenon using an extension of the Laplace transform known as the Z transform [Harrison and Bollinger 1969]. We will not do this here as the procedure is quite involved and beyond the scope of the present work. However, we will use the numerical simulation to examine the sampling phenomenon. The maximum rate for the physical setup was 3.33 samples per second, which is quite low. Since the completion of this project, improvements in software have increased this by about an order of magnitude, so much better control is now possible.

The controllers used in the physical model are highly nonlinear. The describing function concept allows us to apply the Nyquist procedure to such a system. When a

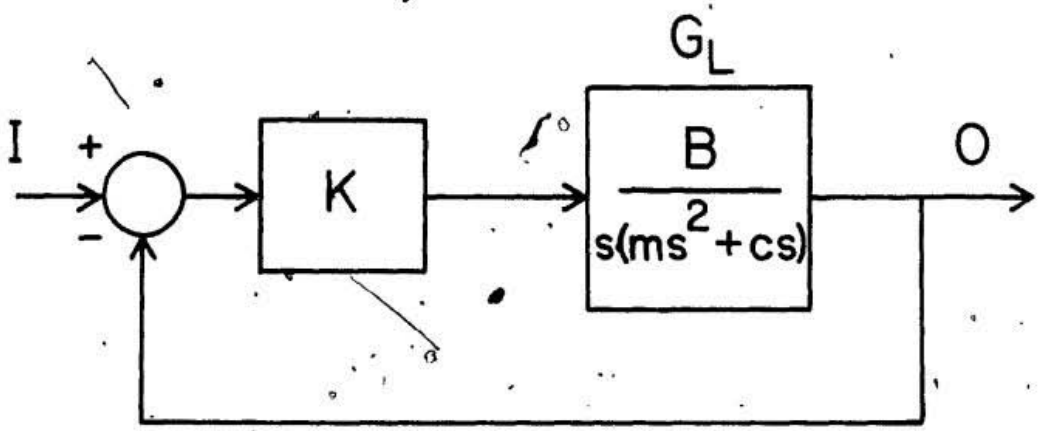


Figure 12 Block Diagram for Capsule with Integral Control.

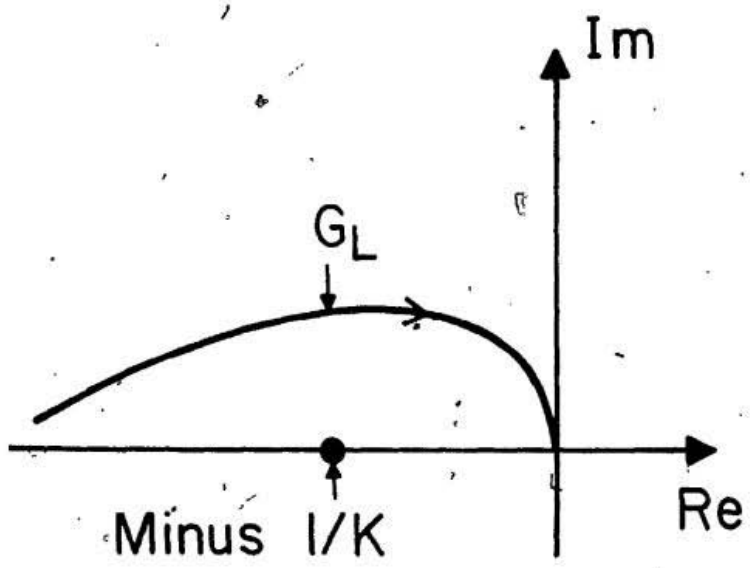


Figure 13 Nyquist Plot for Capsule with Integral Control.

nonlinear system is unstable, nonlinearities usually limit the amplitude of the oscillations which develop to some finite level.. The system is said to be in a limit cycle. Suppose that our escape capsule was undergoing such an oscillation, and suppose also that the signal being fed back around the loop was a pure sinusoid. If the command signal was zero, then the signal into the controller would be a pure sinusoid:

$$I_N = E \text{ Sin } \omega t \tag{3.9}$$

The signal out would be very complex. However, by Fourier Series analysis, it could be broken down into a fundamental component and an infinite number of harmonics:

$$O_N = O_S \text{Sin } \omega t + O_C \text{ Cos } \omega t + \text{Higher Harmonics} \tag{3.10}$$

The describing function for the controller is an amplitude dependent linear element which for the input

$$I_{DF} = E \text{ Sin } \omega t \tag{3.11}$$

gives the output

$$O_{DF} = O_S \text{ Sin } \omega t + O_C \text{ Cos } \omega t \tag{3.12}$$

In other words, its output matches the fundamental component

of the controller's output: it ignores higher harmonics. Manipulations give for the describing function N

$$N = \frac{O_{DF}}{I_{DF}} = \frac{O_S + O_C j}{E} \qquad (3.13)$$

The assumption that the signal fedback is a pure sinusoid is usually a good one because the linear elements which follow the controller normally act a low pass filter and remove the higher harmonics. The block diagram for the describing function approximation of the nonlinear controller is shown in Figure 14.

Now, N is basically an amplitude dependent gain. So, in the Nyquist Plot, the minus 1/N curve must lie to the left of the $G_L$ curve for stable operation. If it lies to the right, the system is unstable. Intersections of the two curves indicate that limit cycles exist [Harrison and Bollinger 1969].

As an illustration, consider a capsule where the rate at which air enters or leaves the central chamber is extremely high. In this case, the density ratio $\Delta$ would jump back and forth from 1.05 to 0.95. The controller would approximate the ideal relay device shown in Figure 15. The describing function for such a device is [Harrison and Bollinger 1969]:

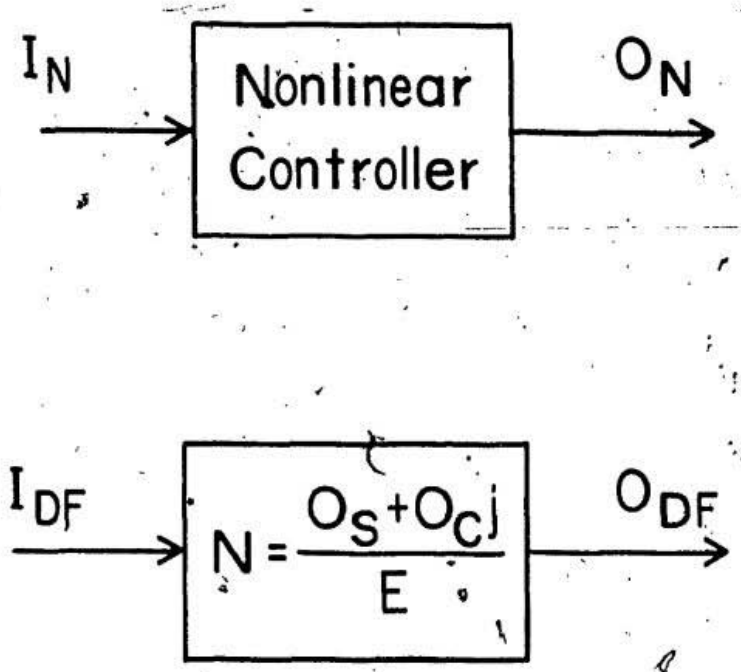


Figure 14 Describing Function Approximation of Nonlinear Controller.

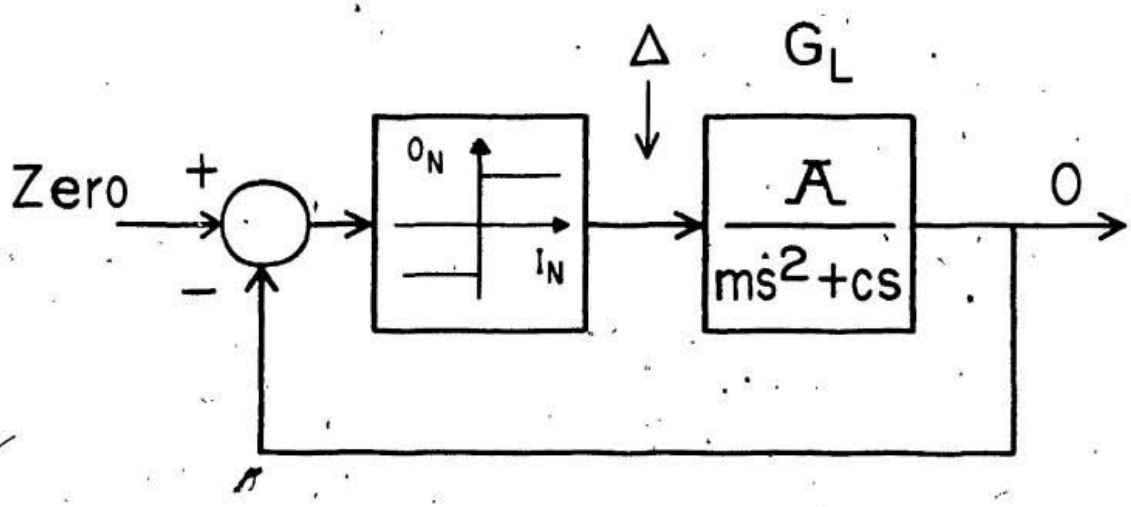


Figure 15 Block Diagram for Capsule with Ideal Relay Density Ratio Controller.

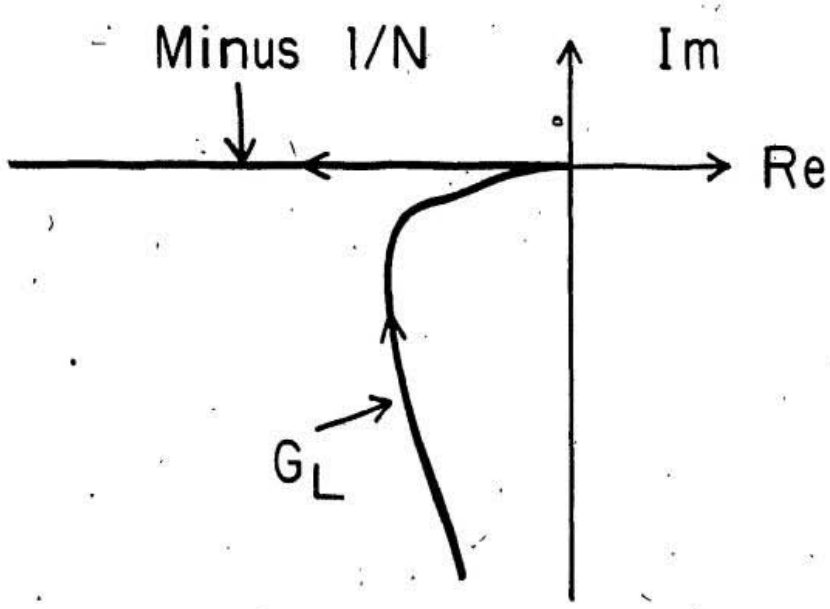


Figure 16 Nyquist Plot for Ideal Relay Density Ratio Controller Case.

$$N = \frac{4A}{\pi E} \qquad (3.14)$$

where E is the limit cycle amplitude and A is the buoyancy force corresponding to $\Delta = 0.05$. The Nyquist plot for this system is shown in Figure 16. The arrow on the minus 1/N curve indicates the direction of increasing E, and the arrow on the $G_L$ curve indicates the direction of increasing $\omega$. As can be seen, the minus 1/N curve lies to the left of the $G_L$ curve and so the system is stable.

There is an intersection at the origin. However, for this limit cycle, E=0 and $\omega=\infty$. For all E greater than zero, minus 1/N is to the left of the $G_L$ curve. Because of this, all system trajectories decay towards the limit cycle at the origin and the limit cycle itself is said to be stable.

Consider now the case where the air flow rates are so low that the limits on the density ratio are never reached. Assume also that rates in and out are constants and equal in magnitude. In this case, the block diagram and the Nyquist plot are as shown in Figures 17 and 18. Note that here A is the magnitude of the flow not the density ratio. As can be seen, the minus 1/N curve lies to the right of the $G_L$ curve. So, the system is unstable. The ideal relay flow adds an extra integration relative to the ideal relay density ratio and this integration makes the system unstable. Again,

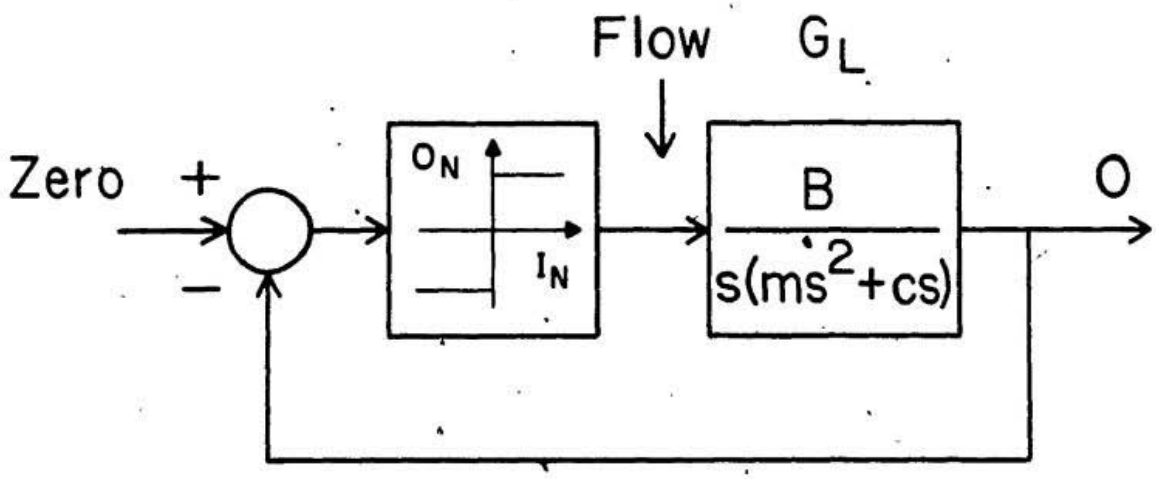


Figure 17 Block Diagram for Capsule with Ideal Relay Flow Controller.

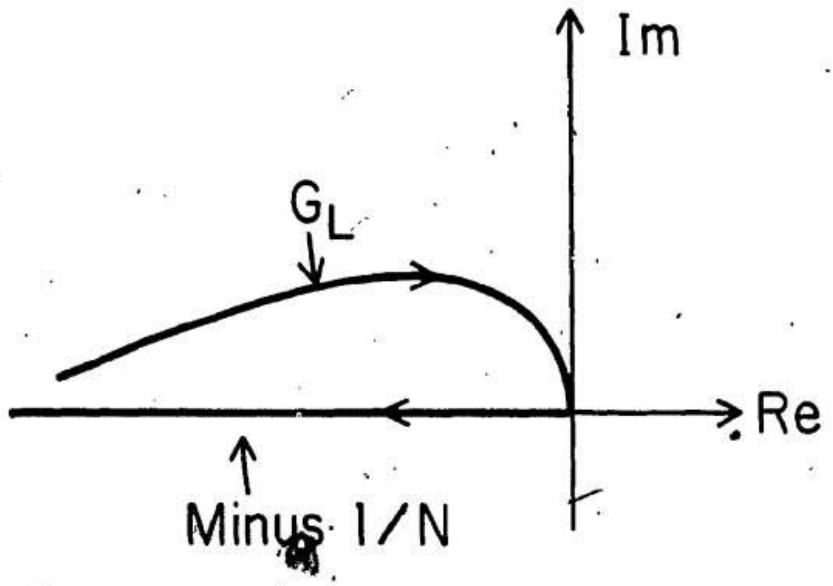


Figure 18 Nyquist Plot for Ideal Relay Flow Controller Case.

there is a limit cycle at the origin. There is also one at infinity where $E=\infty$ and $\omega=0$. The one at the origin is said to be unstable in this case because all trajectories diverge from it while the one at infinity is stable (Figure 19).

An input-output diagram for the second control strategy looks something like that shown in Figure 20. The describing function in this case is

$$N = \frac{4A}{\pi E} j \quad \text{for} \quad E<d \tag{3.15}$$

$$N = \frac{4A}{\pi E}\left[\frac{d}{E} j + \sqrt{1 - \left(\frac{d}{E}\right)^2}\right] \quad \text{for} \quad E>d$$

When the output of the controller is the density ratio, then the Nyquist Plot is as shown in Figure 21. When the output is the flow rate, then it is as shown in Figure 22. In both cases, there is a stable limit cycle at the origin. It appears that the derivative nature of the controller has a stabilizing influence. One drawback of derivative control is it acts only on the rate of change of error. Thus, the error itself can be large and the accuracy of the controller poor.

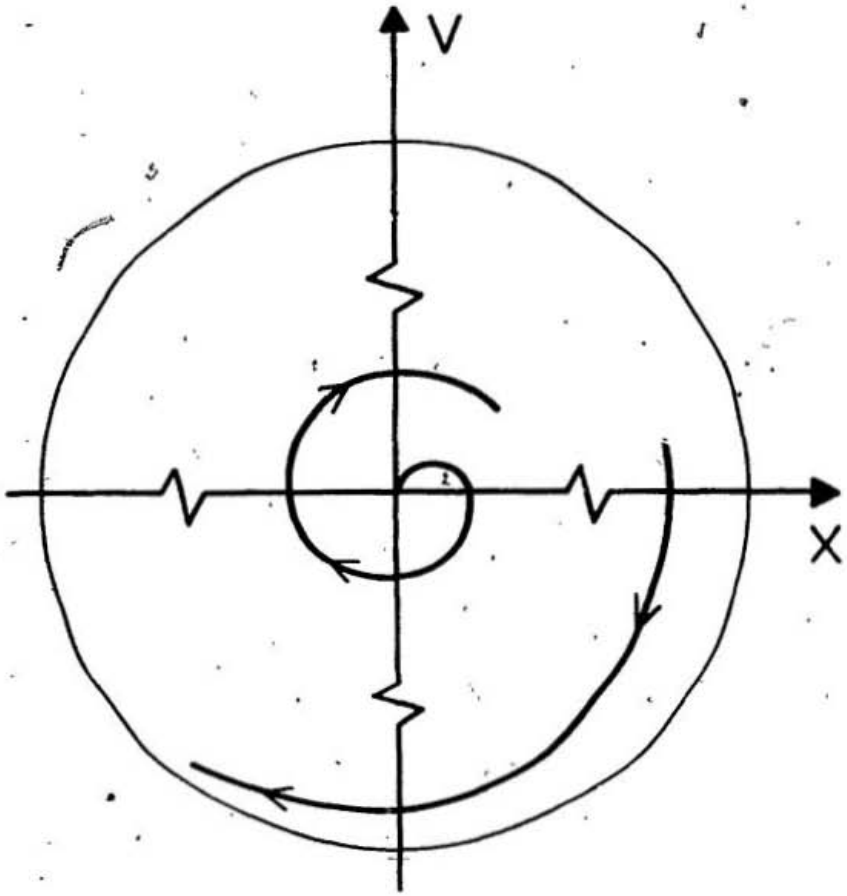


Origin : Unstable

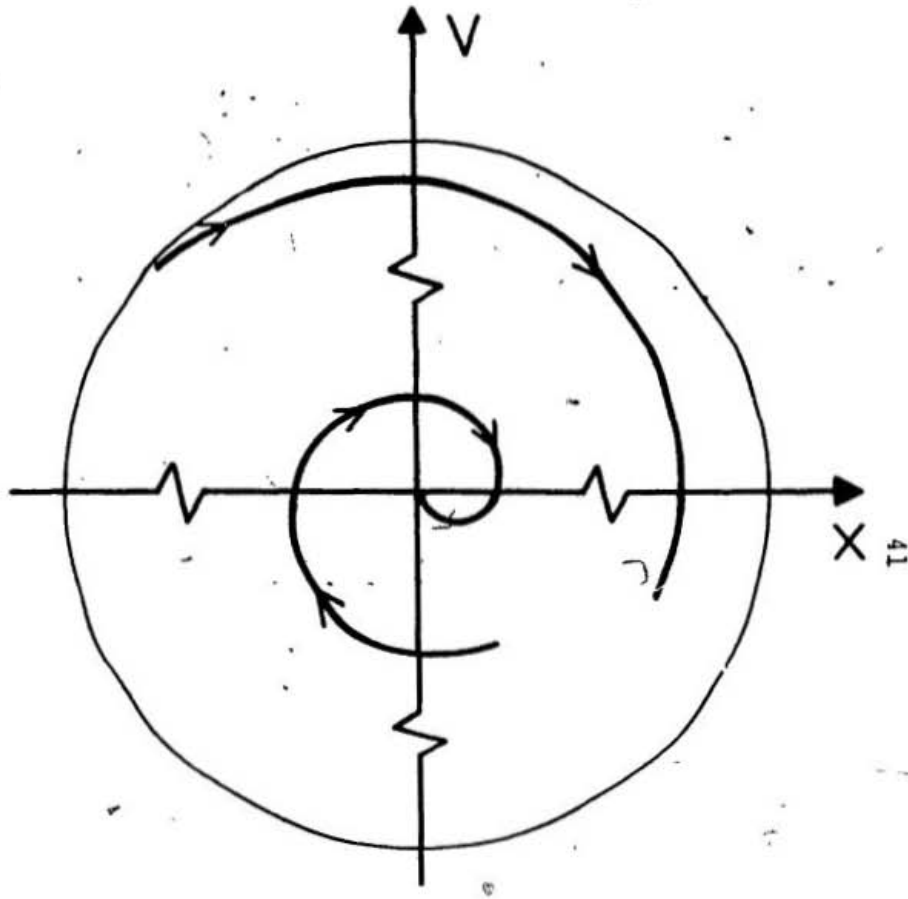


Origin : Stable

Figure 19. Phase Plane Portrait

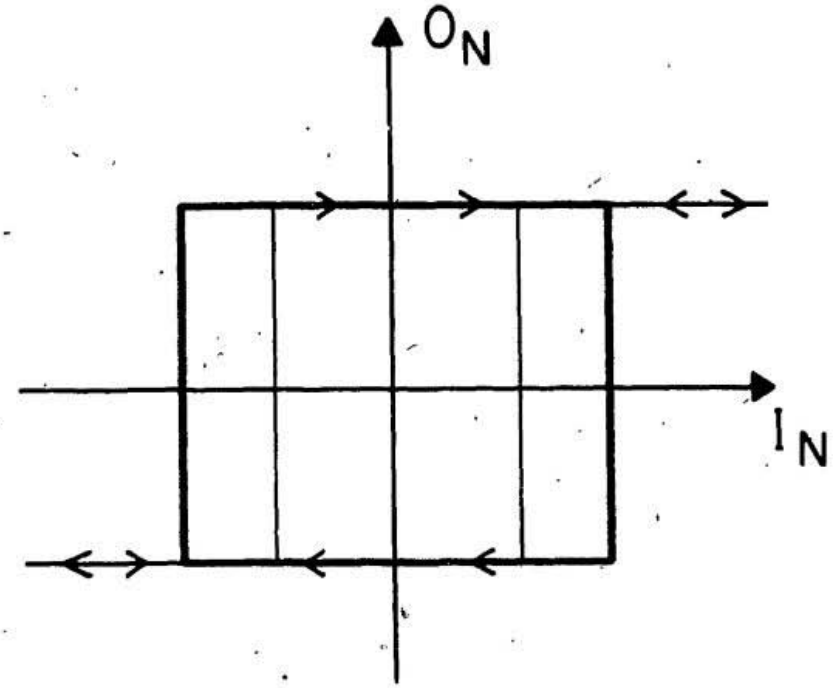


Figure 20 Input-Output Diagram for Second Control Strategy.

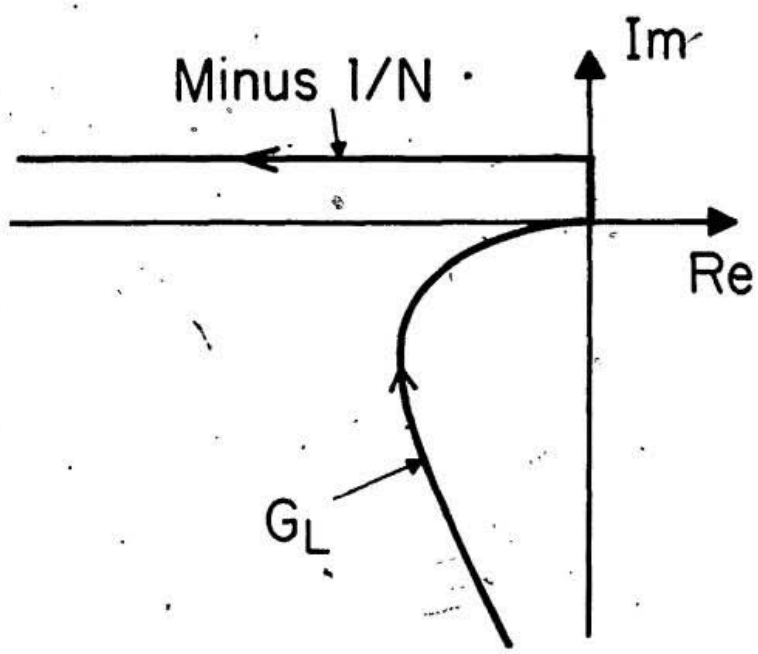


Figure 21 Nyquist Plot for Second Control Strategy with Density Ratio as Output.

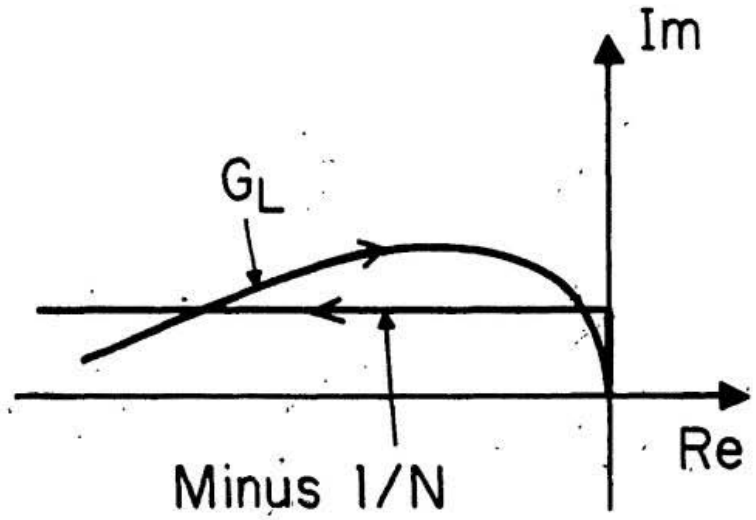


Figure 22 Nyquist Plot for Second Control Strategy with Flow as Output.

### 3.3.3 Numerical Simulation

For the numerical simulation, the governing equations were integrated numerically using a fourth order Runge-Kutta procedure. The initial state, $(Z_o, U_o)$, was set and the solution was marched forward step by step in time.

Figure 23 shows some depth versus time plots generated by the simulation for a case where the controller set the density ratio $\Delta$ to 1.05 if the depth was above 2 m and to 0.95 if it was below 2 m. The initial conditions were $Z_o$=1.9 m, $U_o$=0.25 m/s and $\Delta$=0.99. Describing function theory for this case suggests that it should be stable.

However, in reality, it exhibits limit cycle behaviour. Note that the amplitude of the limit cycle is strongly dependent on the sampling rate SR. As the sampling rate increases, the amplitude becomes smaller and the oscillation frequency increases. It appears that the behaviour is tending towards the zero amplitude infinite frequency limit cycle suggested by the describing function theory.

Figure 24 shows some plots of depth versus time for a case where the controller, acting on the depth error, set the air flow rate in an ideal relay fashion. Also, for the simulation, upper and lower limits on density ratio $\Delta$ were set at 1.05 and 0.95 respectively. The plots show that

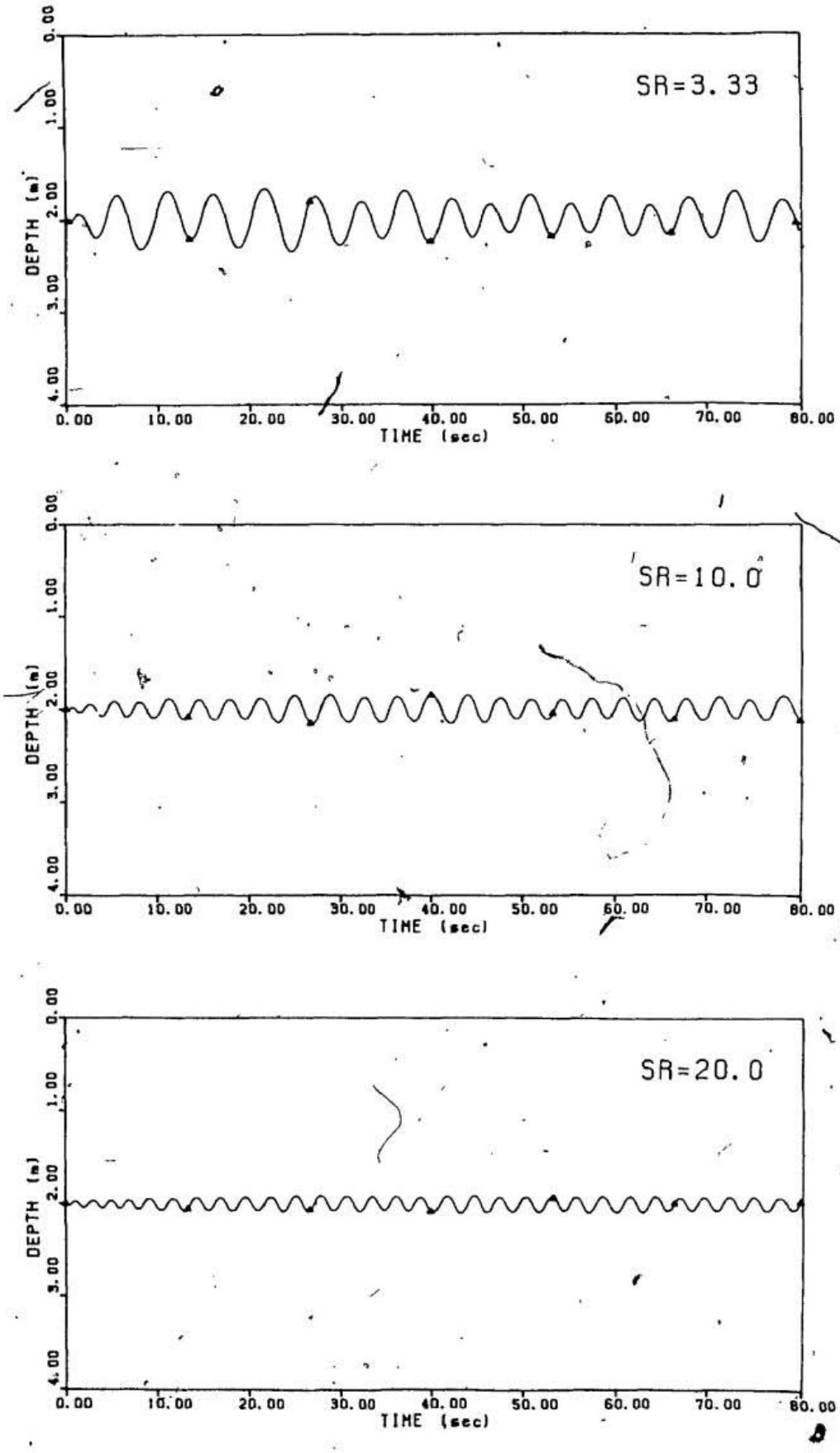


Figure 23 Numerical Simulation Plots for Capsule with Ideal Relay Density Ratio Control.

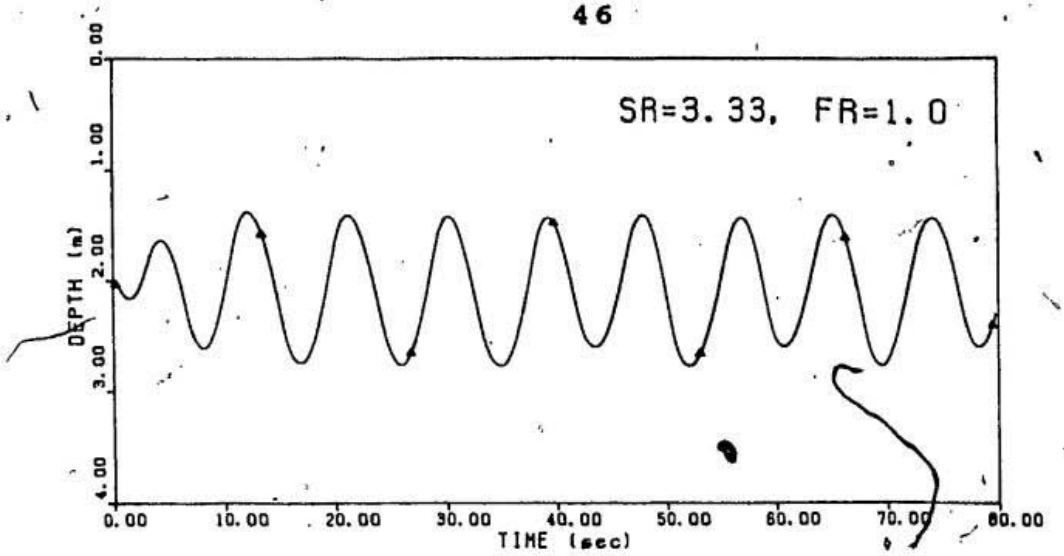


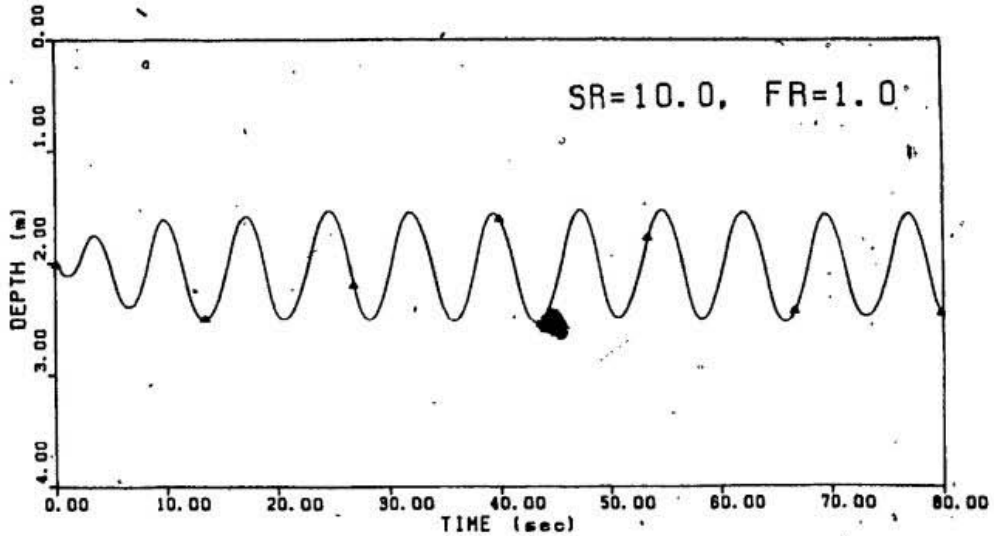


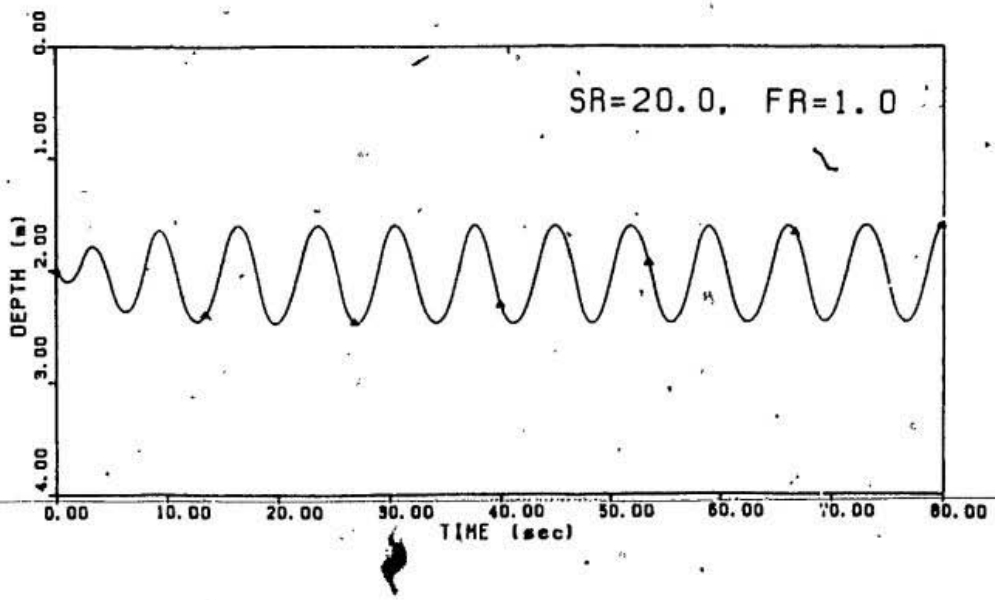


Figure 24 Numerical Simulation Plots for Capsule with Ideal Relay Flow Control with Upper and Lower Limits on Density Ratio.

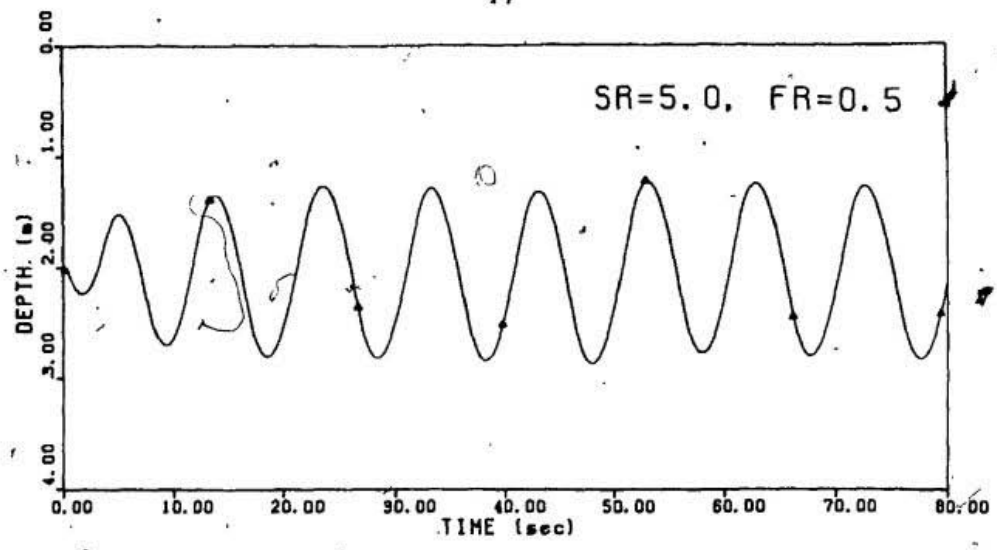
SR=5.0, FR=0.5
DEPTH (m)
0.00
1.00
2.00
3.00
4.00
0.00
10.00
20.00
30.00
40.00
50.00
60.00
70.00
80.00
TIME (sec)

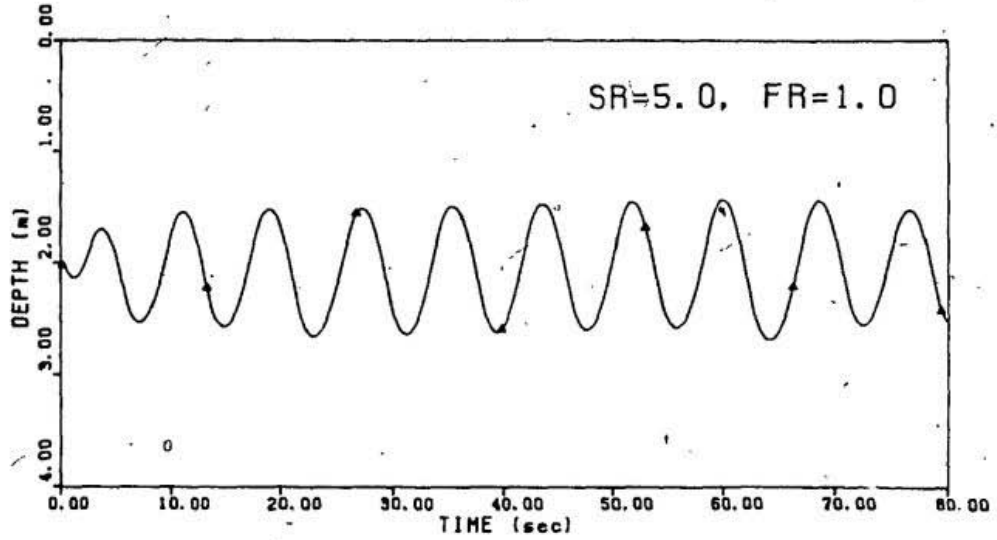
SR=5.0, FR=1.0
DEPTH (m)
0.00
1.00
2.00
3.00
4.00
0.00
10.00
20.00
30.00
40.00
50.00
60.00
70.00
80.00
TIME (sec)

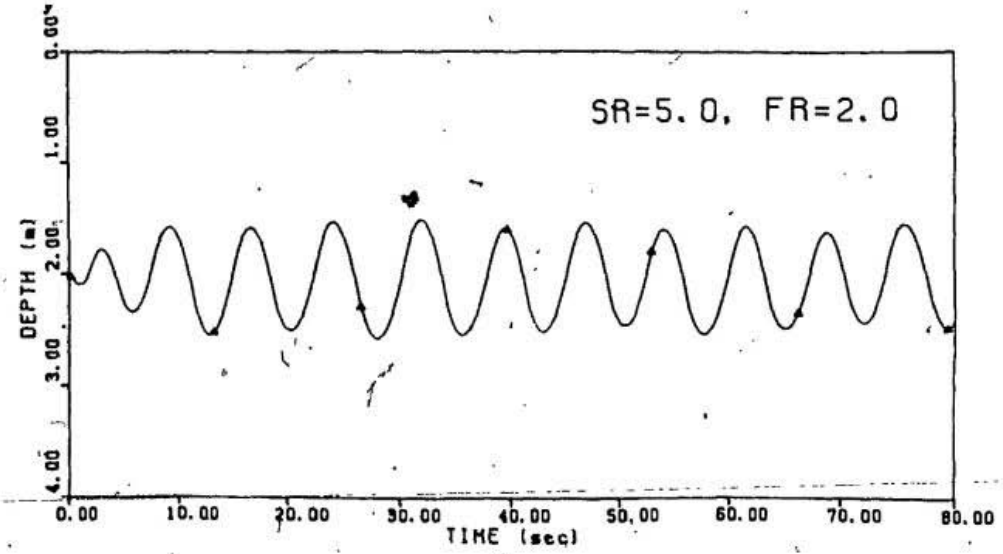
SR=5.0, FR=2.0
DEPTH (m)
0.00
1.00
2.00
3.00
4.00
0.00
10.00
20.00
30.00
40.00
50.00
60.00
70.00
80.00
TIME (sec)

limit cycle behaviour is more pronounced. Describing function theory shows that this is due to the system integration associated with flow. Note, however, that as the sampling rate SR and the flow rate FR both increase, the amplitude of the limit cycle decreases. Again, it appears that the behaviour is tending towards the zero amplitude infinite frequency limit cycle noted earlier.

Figure 25 shows plots for a case where the depth and the direction of motion were both taken into consideration by the controller. Above 1.8 m, the density ratio was set to 1.05. Below 2.2 m, it was set to 0.95. However, within the above range, the direction of motion was taken into consideration. If the capsule was moving upwards within the range, the density ratio $\Delta$ was set to 1.05. If it was moving downward, $\Delta$ was set to 0.95. As can be seen, the stability characteristics are improved. The derivative nature of the control within the range is probably responsible for this. It counteracts the integration in the $G_L$ function. However, the accuracy of the controller is poor because it does not respond to the depth error itself within the range. When the controller gives out flow instead of density ratio, then stability is degraded. Figure 26 shows plots for this case. Again, the system integration associated with flow is probably responsible for this.

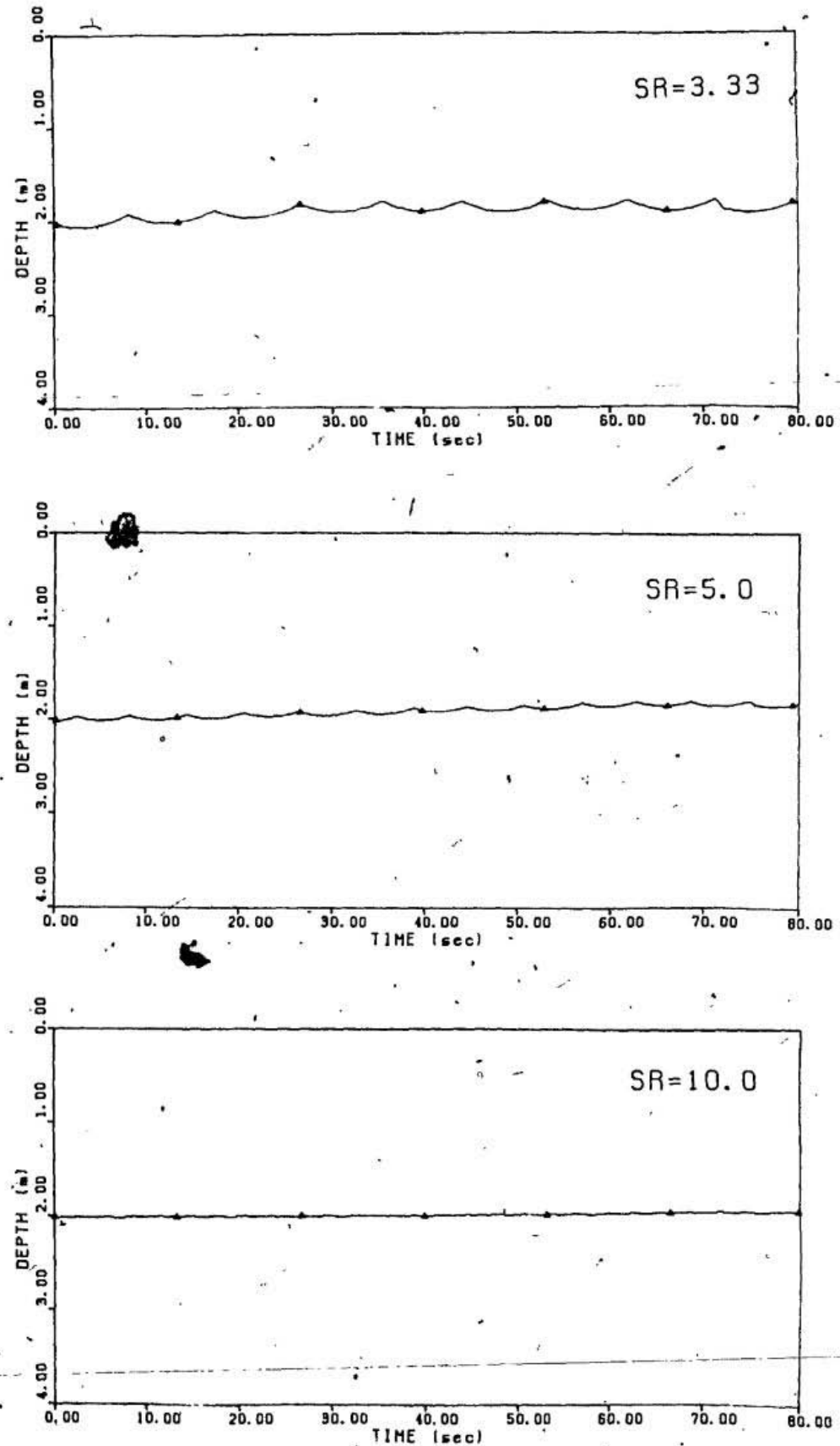


Figure 25 Numerical Simulation Plots for Second Control Strategy with Density Ratio as Output.

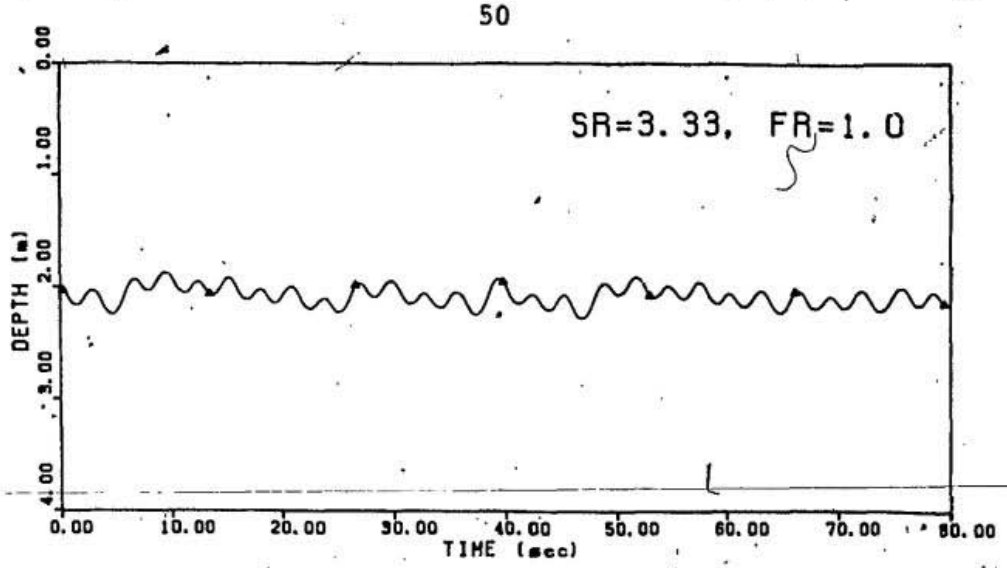


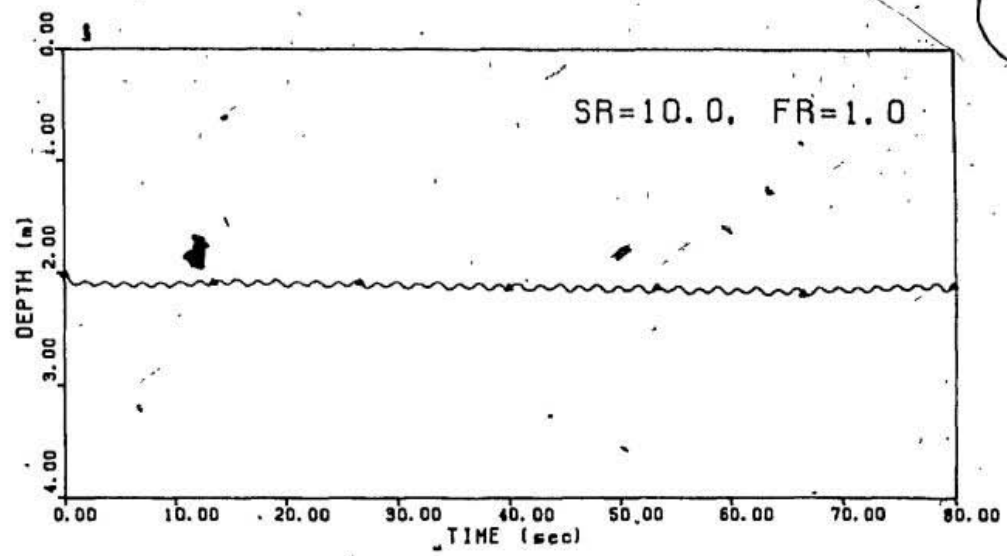


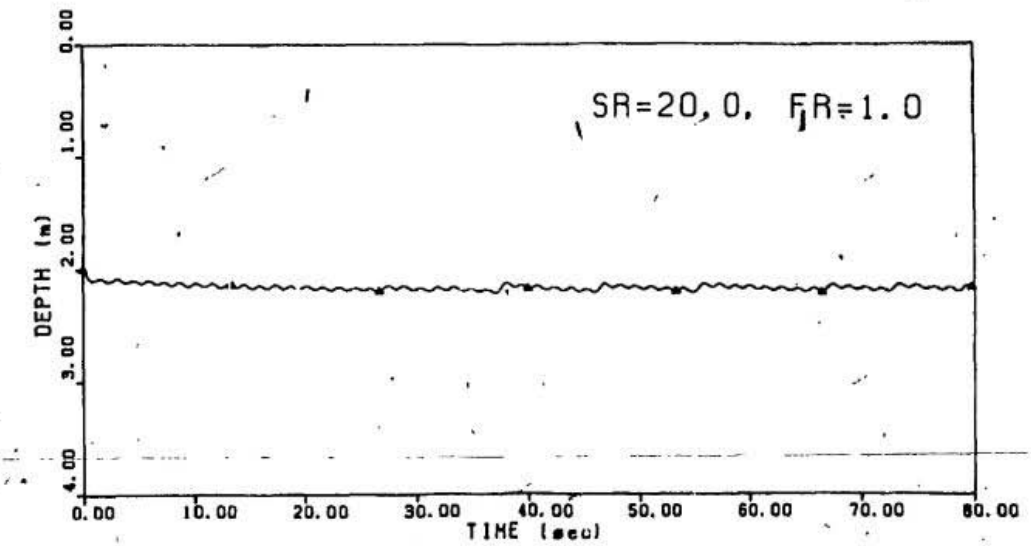


Figure 26 Numerical Simulation Plots for Second Control Strategy with Flow as Output.

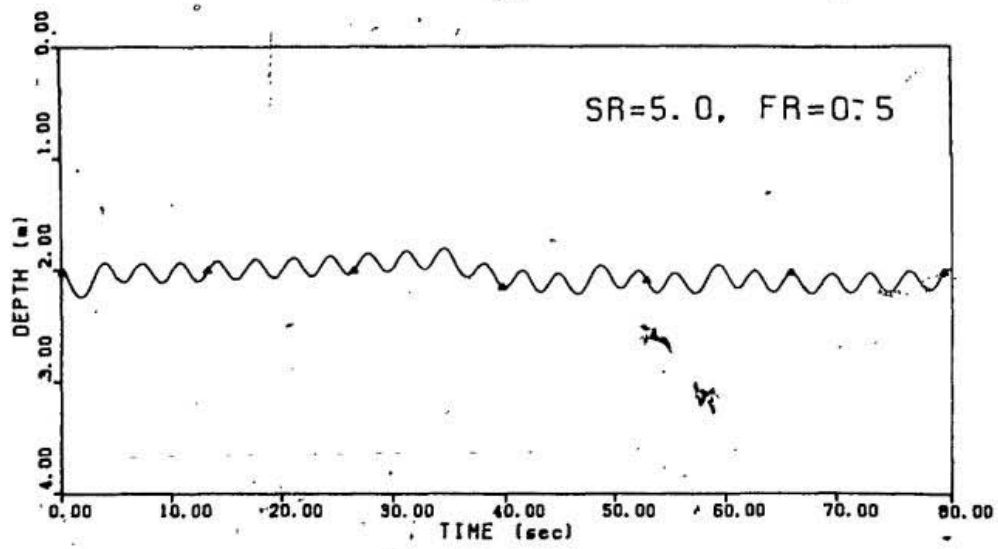
SR=5.0, FR=0.5
DEPTH (m)
0.00
1.00
2.00
3.00
4.00
0.00
10.00
20.00
30.00
40.00
50.00
60.00
70.00
80.00
TIME (sec)

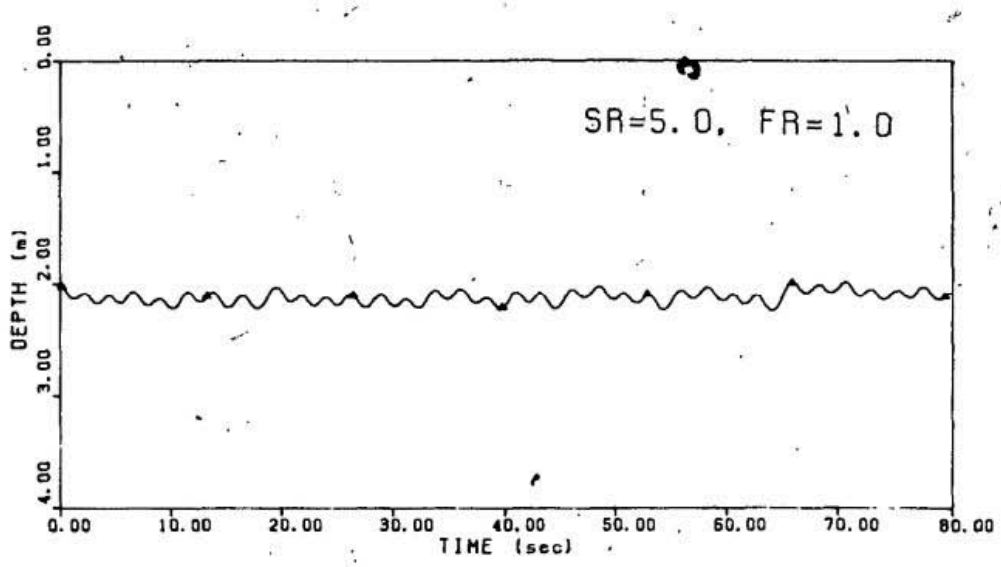
SR=5.0, FR=1.0
DEPTH (m)
0.00
1.00
2.00
3.00
4.00
0.00
10.00
20.00
30.00
40.00
50.00
60.00
70.00
80.00
TIME (sec)

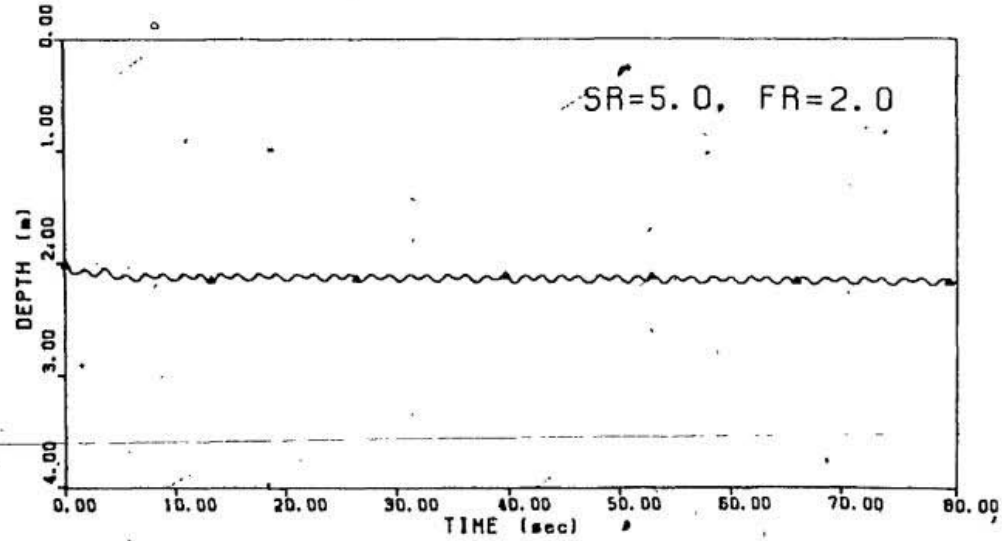
SR=5.0, FR=2.0
DEPTH (m)
0.00
1.00
2.00
3.00
4.00
0.00
10.00
20.00
30.00
40.00
50.00
60.00
70.00
80.00
TIME (sec)

## 3.3 Experimental Data

The density ratio and flow control strategies studied above represent ideals. They only approximate the strategies used in the physical model. This is due mainly to the complex nature of the air supply system.

The first control strategy tested experimentally sent flow into the model when the model depth was below 2 m and allowed flow to vent to atmosphere when the model was above 2 m. Figure 27 shows some depth versus time traces generated in this case. As can be seen, performance is very poor. A large amplitude limit cycle is generated. Adding fins to the model to increase its drag improved things a bit, but not all that much. The sampling and data reconstruction rate for the experiment was 3.33 samples per second. The numerical simulation showed that this rate is too low. In other words, the poor performance is due mainly to the low sampling rate.

The second control strategy tested took into account the model's direction of motion within a depth range centered around the desired depth. For depths below the range, airflow was sent into the model. For depths above, it was allowed to vent to atmosphere. Within the range, air was supplied to the model when it was moving downward, and it was vented to atmosphere when the model was moving

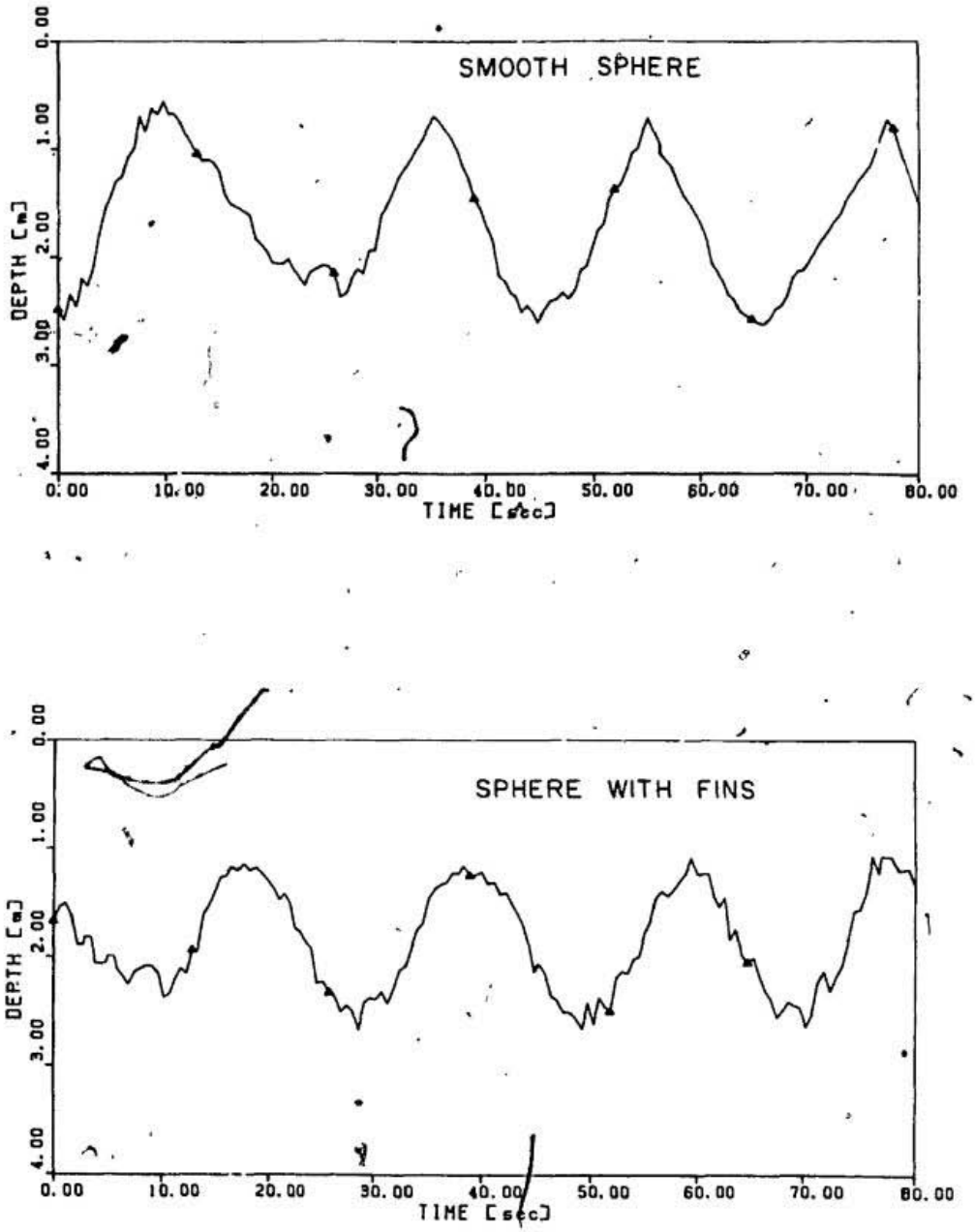


Figure 27 Experimental Data generated by First Control Strategy.

upward. Figure 28 shows typical depth versus time traces generated in this case. Here, the stability characteristics are improved somewhat. However, there is a tendency for the model to drift within the range where the second control strategy is used. Both of these things are probably due to the derivative nature of the controller. However, differences between the inflow and outflow characteristics of central chamber may also be important in this regard.

Figure 29 shows the depth versus time trace generated when the model was allowed to free fall from a height of 1 m above the water surface. The second control strategy was used, again with goal of making the model hover 2 m below the water surface. For a prototype 4.5 m in diameter, this corresponds to a drop from 15 m above the water surface to a depth of 30 m. Figure 30 shows a simulated response for this case. Conditions, following an actual impact, at 0.3 m below the water surface were used to set the initial conditions for the simulation. As can be seen, the agreement between theory and experiment is quite good, and the control is adequate.

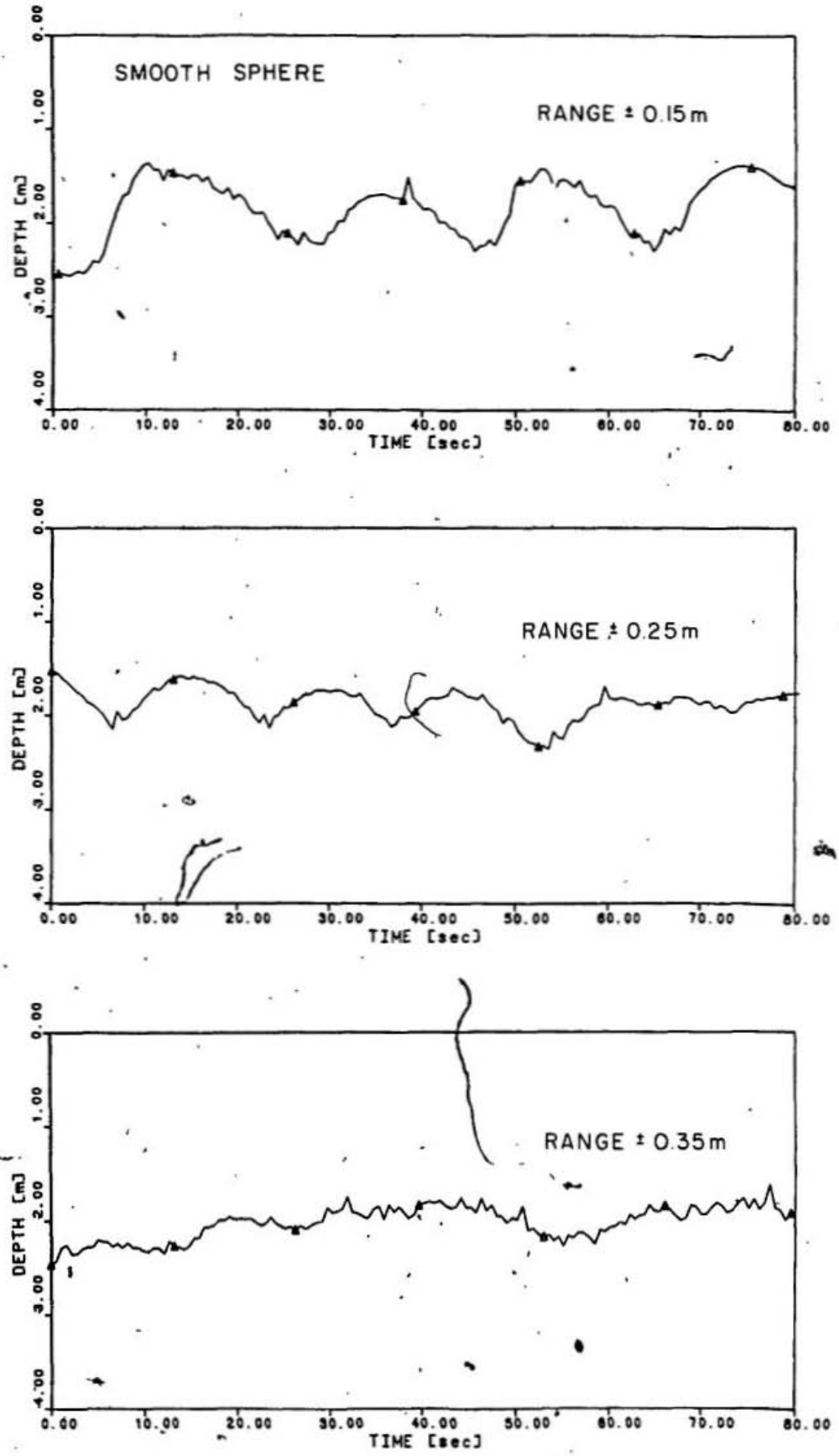


Figure 28* Experimental Data generated by Second Control Strategy.

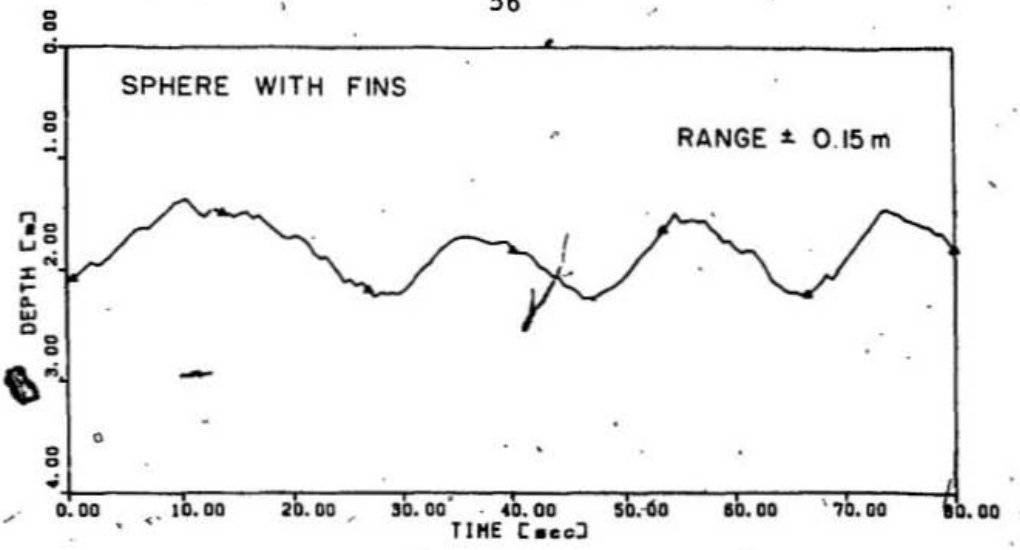
SPHERE WITH FINS
RANGE ± 0.15 m
DEPTH [m]
0.00
1.00
2.00
3.00
4.00
0.00
10.00
20.00
30.00
40.00
50.00
60.00
70.00
80.00
TIME [sec]

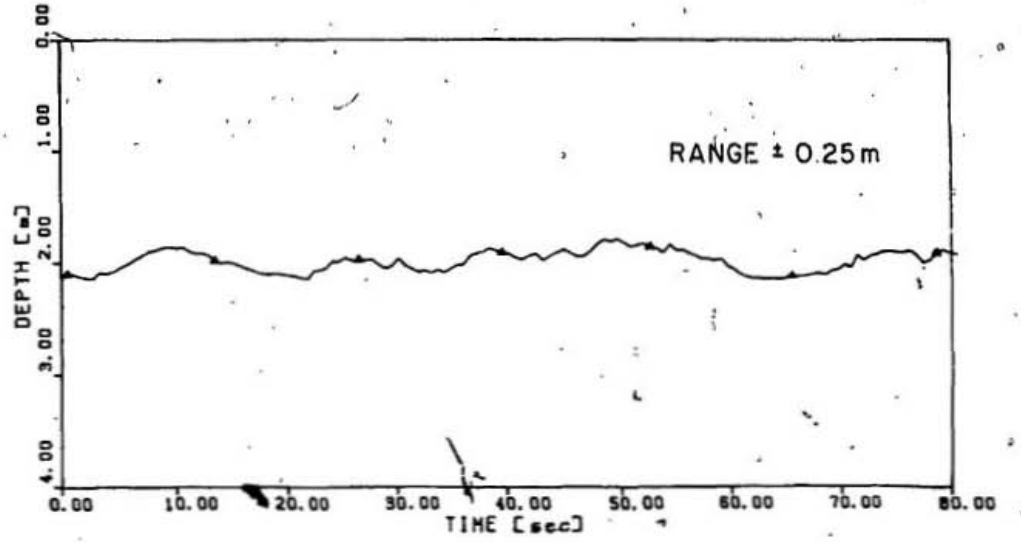
RANGE ± 0.25 m
DEPTH [m]
0.00
1.00
2.00
3.00
4.00
0.00
10.00
20.00
30.00
40.00
50.00
60.00
70.00
80.00
TIME [sec]

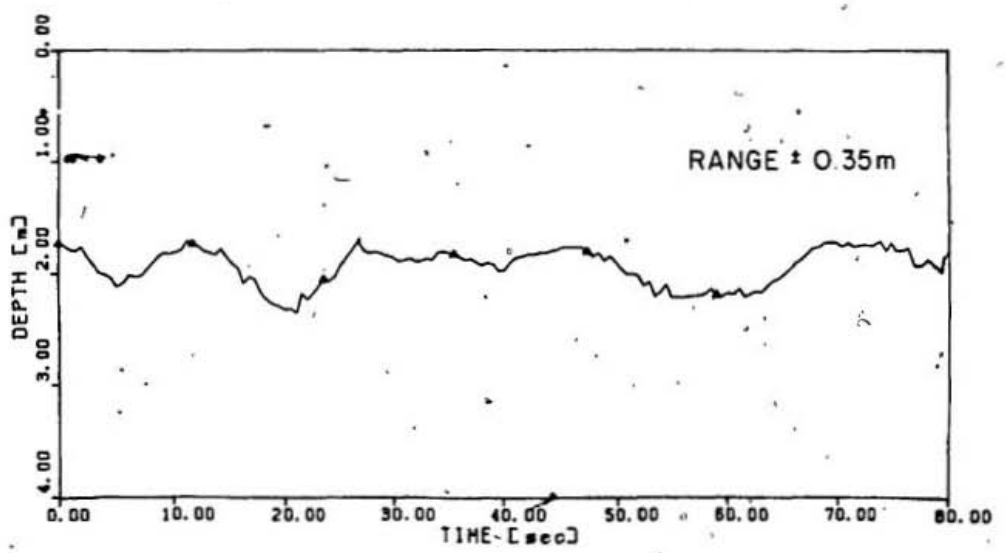
RANGE ± 0.35m
DEPTH [m]
0.00
1.00
2.00
3.00
4.00
0.00
10.00
20.00
30.00
40.00
50.00
60.00
70.00
80.00
TIME [sec]

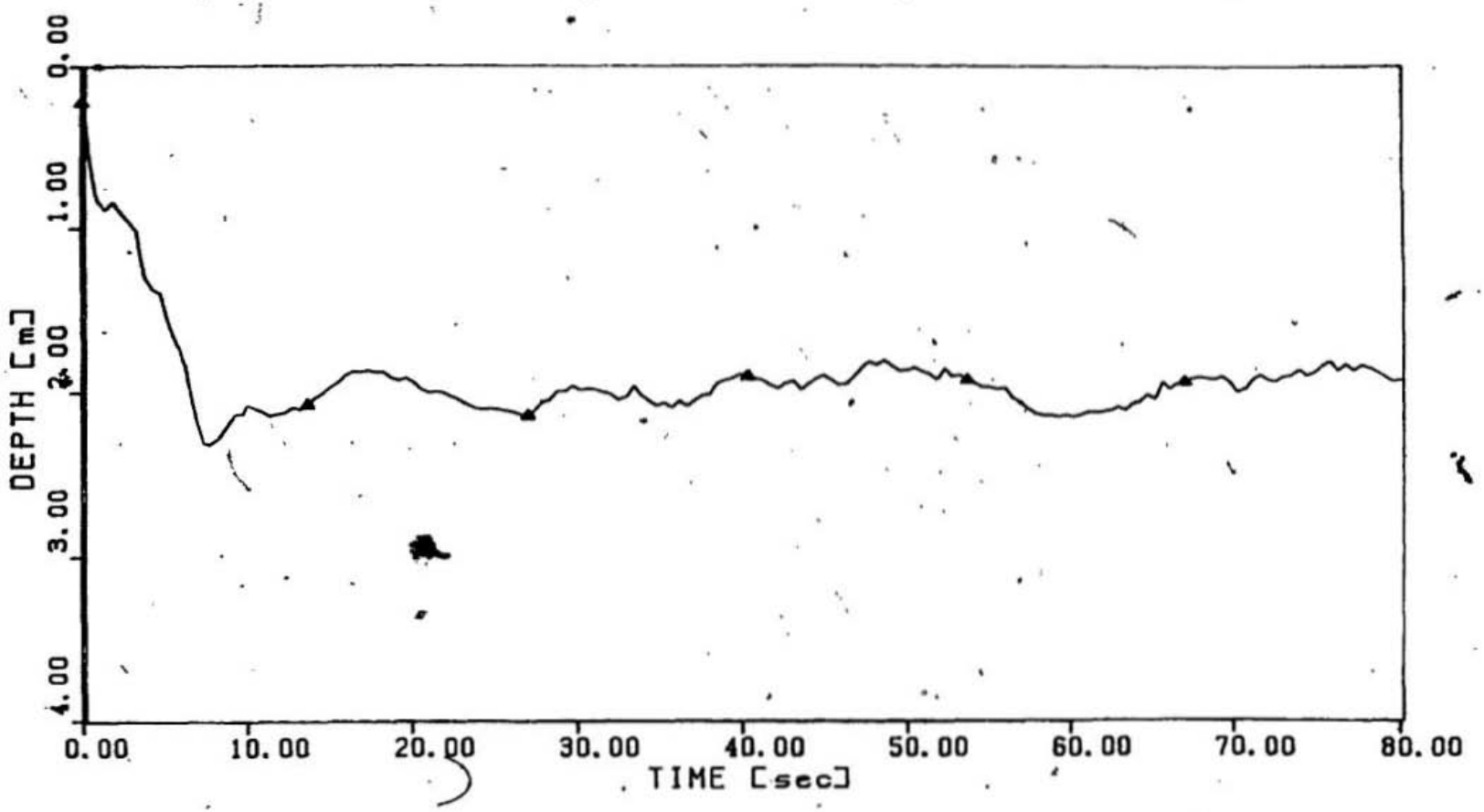


Figure 29 Experimental Data for a Model Free-Fall from 1 m.

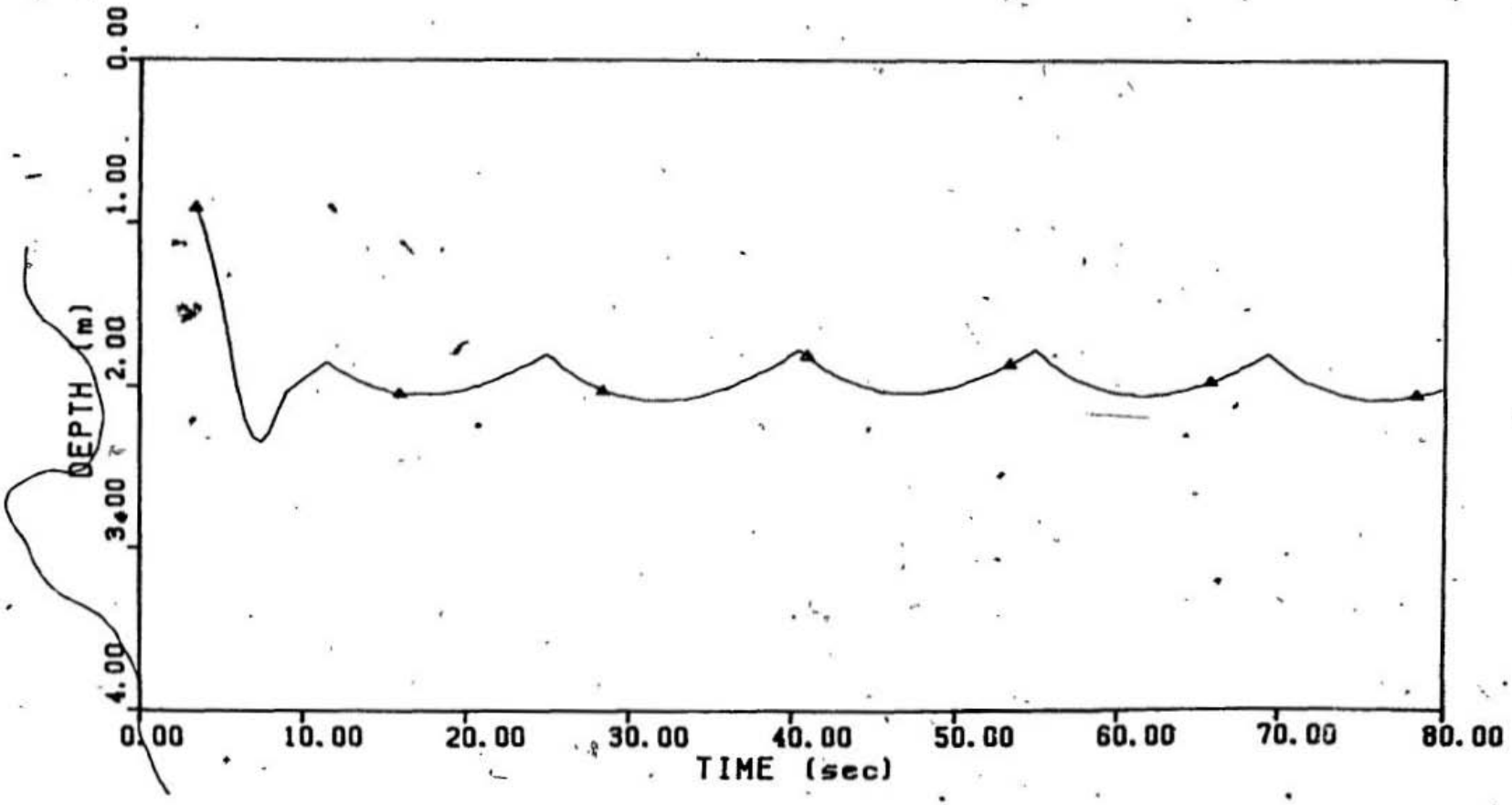


Figure 30 Numerical Simulation of a-Model Free-Fall from 1 m.

## 4. CONCLUSIONS

Recent oil rig disasters have shown that the evacuation systems currently in use offshore are often inadequate during severe storms. Typically, during deployment, survival craft are often damaged to the point of not being seaworthy. In this thesis, a free-fall submersible escape capsule was proposed which, when properly developed, should be able to avoid most of the problems of the present systems. This capsule would free-fall to the ocean surface. It would then sink into the ocean and thus avoid the violent air and water motions near the surface. Two aspects of the proposed systems were studied in detail. Those were the impact of the capsule onto the ocean surface and the control of its submergence depth.

Experiments with spherical models showed that the impact decelerations are well within human tolerance limits. Also, it appears that, for the impact phenomenon, Froude number scaling is appropriate.

For the depth control study, two control strategies were tested both theoretically and experimentally. The goal of each was to make the model capsule hover at a certain depth, usually 2 m, below the water surface. For the experiments, a digital computer was used to sense depth error and take corrective action. For the latter, a flow of

air from an external source was used to adjust the bupyancy of the model. The first control strategy used in the experiment sent a flow of air to the model when the model depth was below 2 m and allowed air to vent to atmosphere when the model was above 2 m. The second strategy took account of the model's direction of motion within a depth range centered around 2 m. When the depth was above the range, air was vented; when it was below, air was supplied. Within the range, air was supplied to the model when it was moving downward and air was vented to atmosphere when the model was moving upward. The second control strategy gave better performance and its control was adequate. With better hardware and more sophisticated control algorithms, even better control should be possible. The describing function concept of classical control theory explained much of what was seen in the depth control experiments.

REFERENCES


1. Baker, W.E., Westine, P.S. and Dodge. (1973), "Similarity Methods in Engineering Dynamics", Spartan Books, pp. 231.

2. Boyd, J., editor. (1984), "New Lifeboat Launch System", East Coast Offshore, Publisher: Harrey, J.B., Newfoundland, Canada.

3. Cheun-Yen, C. (1979), "An Introduction to Computational Fluid Mechanics", John Wiley and Sons, U.S.A.

4. Goldstein, S., editor. (1938), "Modern Developments in Fluid Dynamics: Vol. 1", Clarendon Press, England.

5. Harrison, L.H. and Bollinger, J.G. (1969), "Introduction to Automatic Controls", Harper and Row, Publishers, Inc., U.S.A.

6. Keithley. (1984), Systems 570 Operations Manual.

7. Lamb, H. (1932), "Hydrodynamics", Cambridge University Press, England.

8. Li, T. and Sigimura, T. (1967), "Study of Apollo Water Impact; Vol. 1: Hydrodynamic Analysis of Apollo Water Impact", North American Aviation Inc., Space Division, NAS9-4552, G.O.5264.

9. Muggeridge, D.B. (1985), "Survey of Offshore Drilling Unit Evacuation Systems - Volume 1", Canadian Coast Guard.

10. Nichols, B., Hirt, C. and Hotchkiss, R. (1983), "SOLA-VOF: A Solution Algorithm for Transient Fluid Flow with Multiple Free Boundaries", Los Alamos Scientific Laboratory Report LA-8355.

11. Research Institute of Norway. (1984), "Free-Fall Lifeboats for Offshore Production Platforms", Project Report SSB 2.2.

12. Royal Commission on the Ocean Ranger Marine Disaster. (1984), "Report 1: The Loss of the Semisubmersible Drill Rig Ocean Ranger and Its Crew", Ministry of Supply and Services Canada.

13. Sharp, J.J. (1981), "Hydraulic Modelling", Butterworth Publishers Inc., U.S.A.

14. Vaughan, V.L., Jr. (1961), "Landing Characteristics and Flotation Properties of a Re-Entry Capsule", NASA TN D-653.

15. Werenskoid, P. (1983), "Design of Free-Fall Lifeboat Systems", Proceedings of the International Conference on Marine Survival Craft.

16. Worthington, A.M. and Cole, R.S. (1897), "Impact with a Liquid Surface, Studied with the Aid of Instantaneous Photography", Phil. Trans. Roy. Soc., 189A, pp. 137-148.

# Appendix

## Computer Programs

## Real time computer control

## Program structure

```
PROGRAM Real-time-control

DEFINE Display requirements on the Operator's console

DEFINE Data file to record necessary on-line data

CALL Soft500 ROM

BEGIN

WHILE NOT (The-end-of-the-experiment) DO

        BEGIN

        READ feedback data

        PROCESS control algorithm

        WRITE analog signals to controller

        RECORD data in data-file

        UPDATE display

        END

END
```

Control1.dem

REAL TIME COMPUTER CONTROL

[Position algorithm]

```
010' Set the Operator's console
020  CLS:WIDTH 80
030  SCREEN 1
040  LOCATE 15,1: PRINT 'Date ';DATE$
050  LOCATE 15,17: PRINT 'Time ';TIME$
060  LOCATE 13,1: INPUT 'Set reference depth:';SETDEPTH
070  IF SETDEPTH = -999 THEN 620
080' Data file to record necessary on-line data
090  LOCATE 20,1:INPUT 'Enter data file name:';A$
100  OPEN A$ FOR APPEND AS #1
110  TIME$='00:00:00'
120' Initialize
130  I = 0
140  V = 0
150  VA = 0
160' Call Soft500 ROM
170  CALL INIT
180' begin
190' the infinite loop begins at statement 200
200' record data in data file
210  WRITE #1 I,VA,V
220' read (feedback) analog input in actual Engineering units = volts
230' the digital equivalent is stored in the variable 'VA'
240  CALL ANREAD'('volts1',VA,0)
250' analog to digital conversion completed
260' convert to desired units of depth in meters,
270' using calibration equation of the pressure transducer.
280  DEPTH = (VA/1.4)- 1.5357
290' update display
300  LOCATE 7,14: PRINT TIME$
310  LOCATE 10,12: PRINT I; 'counts'
320  LOCATE 1,1: PRINT '*'
330  LOCATE 1,3: PRINT DEPTH; 'meters'
340  DEPTHNEW = DEPTH
350' begin control strategy [POSITION ALGORITHM]
360  IF DEPTH > SETDEPTH  THEN 490
370  IF DEPTH < SETDEPTH  THEN 400
380' end control strategy
390  DEPTHOLD = DEPTHNEW
400' the desired voltage to relay = zero volts [valve =OFF]
410  V = 0
```

```
420  CALL ANWRITE'('volts2',V,0)
430' digital to analog conversion completed
440' update display
450  LOCATE 4,1:PRINT 'Volts written to channel zero =';V
460  LOCATE 1,1:PRINT ' '
470  I = I + 1
480  I$ = INKEY$:IF I$='' THEN 200 ELSE 580
490' the desired voltage to relay = five volts [valve =ON]
500  V = 5
510  CALL ANWRITE'('volts2',V,0)
520' digital to analog conversion completed
530' update display
540  LOCATE 4,1:PRINT 'Volts written to channel zero =';V
550  LOCATE 1,1:PRINT ' '
560  I = I + 1
570  I$ = INKEY$: IF I$='' THEN 200 ELSE 580
580' end procedure ( out of the infinite loop )
590  BEEP:BEEP:BEEP
600  LOCATE 17,1:PRINT 'Print the necessary log'
610  SCREEN 2
620  END
```

Control2.dem

REAL TIME COMPUTER CONTROL

[Velocity algorithm]

```
010' Set the Operator's console
020  CLS:WIDTH 80
030  SCREEN 1
040  LOCATE 15,1: PRINT 'Date ';DATE$
050  LOCATE 15,17: PRINT 'Time ';TIME$
060  LOCATE 13,1: INPUT 'Set reference depth:';SETDEPTH
070  IF SETDEPTH = -999 THEN 620
080' Data file to record necessary on-line data
090  LOCATE 20,1:INPUT 'Enter data file name:';A$
100  OPEN A$ FOR APPEND AS #1
110  TIME$='00:00:00'
120' Initialize
130  I = 0
140  V = 0
150  VA = 0
160' Call Soft500 ROM
170  CALL INIT
180' begin
190' the infinite loop begins at statement 200
200' record data in data file
210  WRITE #1 I,VA,V
220' read (feedback) analog input in actual Engineering units = volts
230' the digital equivalent is stored in the variable 'VA'
240  CALL ANREAD'('volts1',VA,0)
250' analog to digital conversion completed
260' convert to desired units of depth in meters,
270' using calibration equation of the pressure transducer.
280  DEPTH = (VA/1.4) - 1.5357
290' update display
300  LOCATE 7,14: PRINT TIME$
310  LOCATE 10,12: PRINT I; 'counts'
320  LOCATE 1,1: PRINT '*'
330  LOCATE 1,3: PRINT DEPTH; 'meters'
340  DEPTHNEW = DEPTH
350' begin control strategy [VELOCITY ALGORITHM]
360  IF DEPTH > SETDEPTH + 0.15 THEN 530
370  IF DEPTH < SETDEPTH - 0.15 THEN 440
380  IF DEPTH > SETDEPTH AND DEPTHNEW > DEPTHOLD THEN 530
390  IF DEPTH > SETDEPTH AND DEPTHNEW < DEPTHOLD THEN 440
400  IF DEPTH < SETDEPTH AND DEPTHNEW > DEPTHOLD THEN 530
410  IF DEPTH < SETDEPTH AND DEPTHNEW < DEPTHOLD THEN 440
```

```
420' end control strategy
430  DEPTHOLD = DEPTHNEW
440' the desired voltage to relay = zero volts [valve =OFF]
450  V = 0
460  CALL ANWRITE'('volts2',V,0)
470' digital to analog conversion completed
480' update display
490  LOCATE 4,1:PRINT 'Volts written to channel zero =';V
500  LOCATE 1,1:PRINT ' '
510  I = I + 1
520  I$ = INKEY$:IF I$='' THEN 200 ELSE 620
530' the desired voltage to relay = five volts [valve =ON]
540  V = 5
550  CALL ANWRITE'('volts2',V,0)
560' digital to analog conversion completed
570' update display
580  LOCATE 4,1:PRINT 'Volts written to channel zero =';V
590  LOCATE 1,1:PRINT ' '
600  I = I + 1
610  I$ = INKEY$: IF I$='' THEN 200 ELSE 620
620' end procedure ( out of the infinite loop )
630  BEEP:BEEP:BEEP
640  LOCATE 17,1:PRINT 'Print the necessary log'
650  SCREEN 2
660  END
```